First Tests of a Square Wave Radio Frequency Quadrupole Cooler and Buncher for TITAN

Laura Gail Blomeley

Department of Physics

McGill University

Montreal,Quebec

2007-01-14

A thesis submitted to McGill University in partial fulfillment of the requirements of the degree of Master of Science

ACKNOWLEDGMENTS

This project would not have been possible without the support of many people. Many thanks to my advisors at McGill, Jonathan Lee and John Crawford, who read my numerous revisions and helped make some sense of the confusion. I am immensely grateful for the supervision and advice of Jens Dilling and Joe Vaz while working on this research at TRIUMF in Vancouver. Also thanks to the TITAN group at TRIUMF, Mathew Smith, Vladimir Ryjkov, Maxime Brodeur and Mel Good, who were always on hand to answer questions and give advice.

I also wish to thank TRIUMF and the staff I encountered there. I could not have completed this work without the many conversations with people on the varied subjects of power supplies, programming, nuclear structure - and World Cup football.

And finally, thanks to my parents, sister, and numerous friends who endured this long process with me, always offering support and love.

ABSTRACT

A high frequency, large amplitude helium filled RFQ (Radio Frequency Quadrupole) beam cooler and buncher was developed and tested for use in the TITAN (TRIUMF's Ion Trap for Atomic and Nuclear science) Penning trap mass spectrometer facility. This device will cool and bunch radioactive ion beams for use in TITAN's high precision mass measurements of short-lived isotopes and other experiments. A test stand was built to test the transmission and properties of ions from a surface ion source through injection optics, the linear Paul trap RFQ and the extraction optics in both continuous and pulsed modes. The efficiency of the device was determined to be on the order of 60% in continuous mode. The present measurements confirm a transverse emittance of the extracted beam in bunched mode operation of 4 π-mm-mrad at an extraction energy of 4 keV.

RÉSUMÉ

Un quadrupole à fréquences radio (RFQ) a été développé et testé à TITAN (piège à ion pour études atomiques et nucléaires à TRIUMF), le nouveau piège à ion de Penning pour la spectroscopie de masse de haute précision à ISAC (séparateur et accélérateur d'isotopes). Cet appareil fonctionne à hautes fréquences, larges amplitudes et en présence d'hélium. Il vise à refroidir et hâcher le faisceau radioactif pour mesurer avec précision la masse d'isotopes à courte demi-vie et à réaliser d'autres expériences. La transmission et les propriétés d'un faisceau stable produit par une source d'ionisation de surface ont été testées sur un banc d'essai où étaient réunis l'optique d'injection, le piège linéaire de Paul et l'optique d'extraction. Ces tests ont été effectués avec un faisceau continu ainsi qu'avec un faisceau hâché. L'efficacité de l'appareil est de l'ordre de 60% avec le faisceau continu. Avec le faisceau hâché, une émittance longitudinale de $4\pi \cdot \text{mm} \cdot \text{mrad}$ est mesurée pour une énergie d'extraction de 4keV.

TABLE OF CONTENTS

LIST OF TABLES

LIST OF FIGURES

CHAPTER 1
Introduction

The subject of this thesis is the off-line testing and commissioning of the RFQ (Radio Frequency Quadrupole) cooler and buncher designed and built for operation with the TITAN (TRIUMF's Ion Trap for Atomic and Nuclear science) facility at TRIUMF (TRI-University Meson Facility). This beam manipulating and refining device is an essential component in the new high-precision mass measurement facility at TRIUMF. Among the issues examined are the motivation for building the device, its theoretical aspects and its performance in a test setup.

1.1 TITAN at TRIUMF

TRIUMF in Vancouver Canada, is a cyclotron based nuclear research facility. The cyclotron accelerates protons up to an energy of 520 MeV and is used as the driver for production of mesons (π^+, π^-, π^0) and subsequent muons, and for the production of radioactive nuclei in the ISAC (Ion Separator and Accelerator) complex. The ISAC facility separates and accelerates radioactive ions generated when protons impact on a target. These ions can be used in various experiments in the ISAC experimental hall, including TITAN. Figure 1-1 illustrates the layout of the ISAC hall. The TITAN beam line and platform are situated between the polarised beam line and the DTL (Drift Tube Linac) accelerator section.

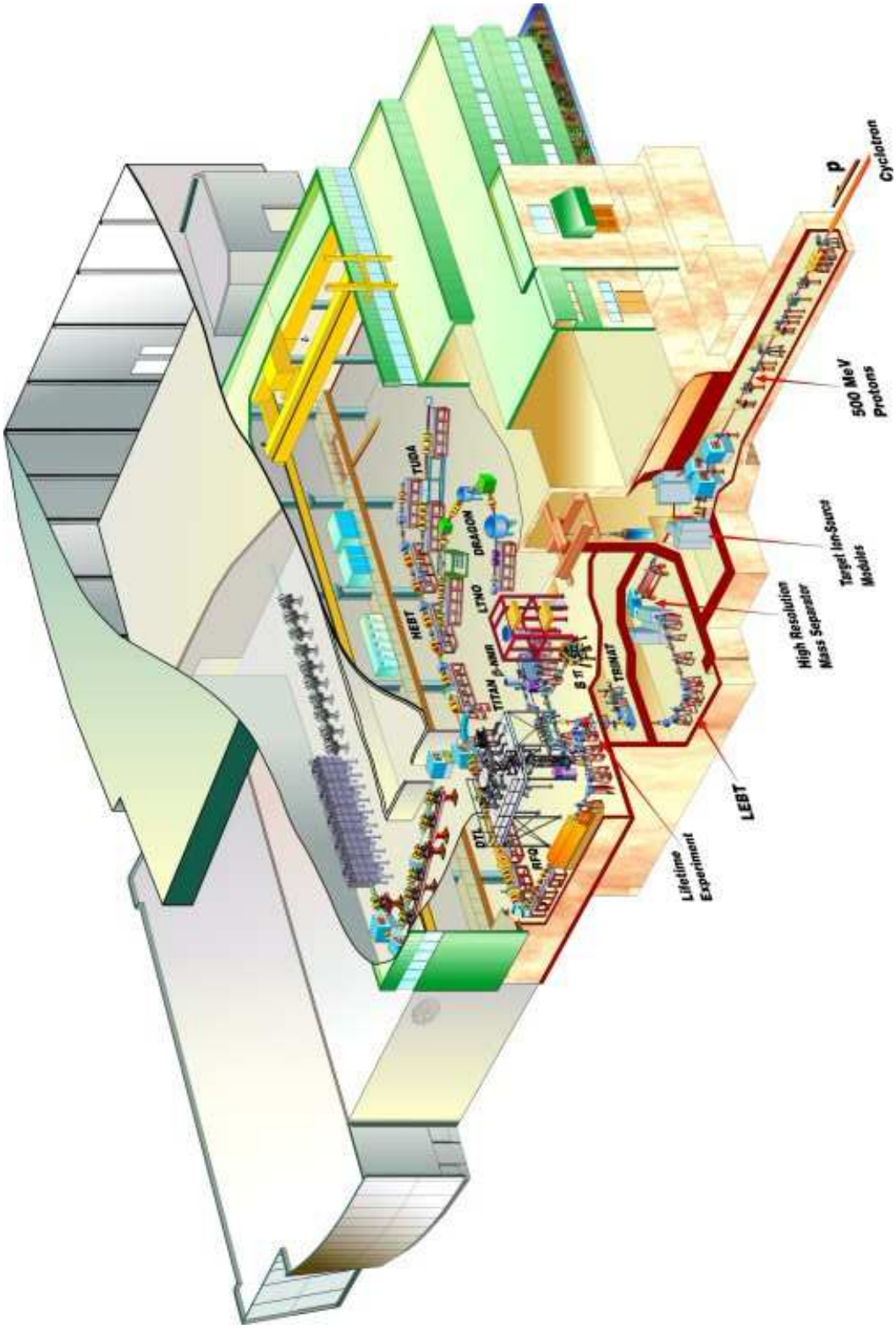

Figure 1–1: The ISAC experimental hall

The ISAC complex at TRIUMF is a radioactive beam facility of the ISOL (Ion Separation OnLine) type with the capability of producing isotopes ultimately up to uranium and delivers mass separated ions of typical energies 30-60 keV to a variety of experiments [1]. The high yield of exotic nuclei that can be produced at ISAC, due mainly to high proton intensities, enables TITAN to carry out mass measurements on isotopes that have not been previously accessible at other facilities. This is also due to the fact that the system includes an EBIT (Electron Beam Ion Trap) charge breeding device which will increase the charge state of the ions. Because the precision of a mass measurement in the Penning trap is dependent on the charge, mass and time in the trap (see section 1.3.1) an increased means less time will be needed to acquire the statistics needed for high precision mass measurements and will allow for the mass determination of shorter lived isotopes ($T_{1/2} \leq 50$ms.)

1.2 The TITAN System

1.2.1 Mass Measurements and Motivation

The TITAN system is primarily a Penning trap mass spectrometer. Measurements of atomic masses are of fundamental importance since they allow the determination of nuclear binding energies in a complex many body system. Their precise determination ($\frac{\delta m}{m} \leq 10^{-7}$) allows one to detect many effects otherwise hidden. This precision corresponds to a Δm of 100 keV for A = 100, far less than the typical binding energy per nucleon ($\approx$ 2-5 MeV). But in general, many areas of nuclear and particle physics benefit from increased precision in mass measurements.

As an example of how increased mass measurement precision can be useful, we look at the CKM (Cabibbo Kobayashi Maskawa) matrix. The CKM matrix dictates the mixing of the weak and strong force eigenstates using the

mixing angles V_{ij} where i and j denote the different quarks:

$$\begin{pmatrix} d_w \\ s_w \\ b_w \end{pmatrix} = \begin{pmatrix} V_{ud} & V_{us} & V_{ub} \\ V_{cd} & V_{cs} & V_{cb} \\ V_{td} & V_{ts} & V_{tb} \end{pmatrix} \cdot \begin{pmatrix} d_s \\ s_s \\ b_s \end{pmatrix} \tag{1.1}$$

In the Standard Model, the matrix is unitary. If it were found to be non-unitary, this would indicate the existence of CP violations in the Standard Model [2] and possibly new physics. Compilations of experimental results and including needed corrections have shown that at the two sigma level

$$M = \begin{pmatrix} 0.9741 \pm 0.0005 & 0.2263 \pm 0.0020 & 0.0039 \pm 0.0002 \\ 0.2261 \pm 0.0020 & 0.9732 \pm 0.0005 & 0.0422 \pm 0.0013 \\ 0.0082 \pm 0.0011 & 0.0416 \pm 0.0013 & 0.9991 \pm 0.0001 \end{pmatrix}, \tag{1.2}$$

yielding for the first row:

$$V_{ud}^2 + V_{us}^2 + V_{ub}^2 = 1.0000 \pm 0.0007[3]. \tag{1.3}$$

While this is equal to unity at the present time, recent measurements have led to corrections (see for example [4] and [5]) and more measurements are needed to ensure that this really is the case. Specifically, the matrix element V_{ud}, when applied to super-allowed beta-emitting nuclei, depends on the mass through the Ft value which relates to the beta decay half-life and energy [6]. For this application, the effect of the mass on the matrix element is small and the precision required on nuclear mass measurements to test this value and determine the unitarity of the CKM matrix is on the order of $\delta m/m \leq 1\text{x}10^{-8}$. The TITAN mass spectrometer combined with the high yields of radioactive isotopes available at ISAC will be able to reach this precision for short-lived isotopes [7].

1.2.2 The TITAN Components

The main components of TITAN are the RFQ (Radio Frequency Quadrupole) buncher and cooler, the EBIT (Electron Beam Ion Trap), and the precision Penning trap. Figure 1-2 shows where each component fits into the experimental setup. Ions will enter the system from the ISAC beam line at TRIUMF, and will be cooled and bunched in the RFQ before transport to the EBIT. The EBIT will use a high energy (up to 60 keV), high current (up to 5 A) [8] electron beam to ionise the singly charged ions to higher charge states. After sufficient ionisation, these highly charged ions will be sent through a Wien filter to separate out unwanted charge states and then be transported to the Penning trap where their masses can be measured. The system is designed to be modular so that experiments can be done with ions from the RFQ or from the EBIT without involving the whole beam line. A schematic of the ion transfers is shown in Figure 1-3.

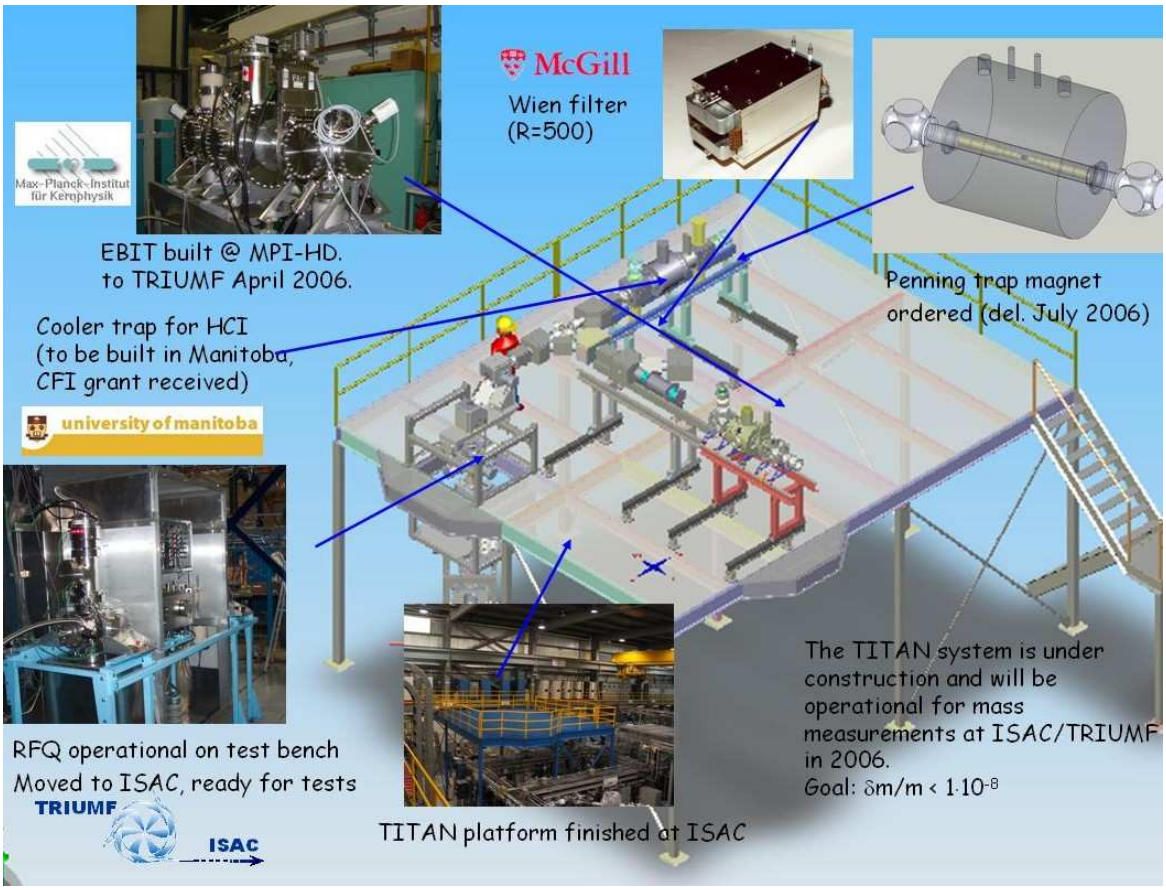

Figure 1–2: The TITAN system at ISAC

The following sections give a more detailed description of the other main components of TITAN: the EBIT, the precision Penning trap and finally the RFQ which is the subject of this thesis.

The EBIT was built and underwent first testing at the Max Planck Institute for Nuclear Physics in Germany. Because the precision depends on both the charge and the duration of the applied RF during measurement, increasing the charge state can yield higher precision measurements for long lived isotopes and and reduce the time required to achieve a certain precision allowing for measurement of shorter lived isotopes. The effect of higher charge states on the measurement times and precision of mass measurements in a Penning trap is shown in Figure 1-4. The precision achieved in a Penning trap measurement

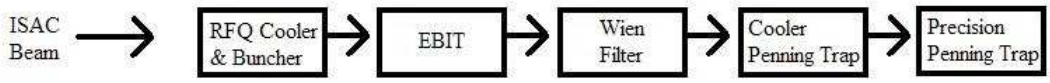

Figure 1–3: Flow diagram of the ion path

of a mass m (see chapter 1.3 of this work) is given by

$$\frac{\delta m}{m} = \frac{m}{T_{RF} \cdot Q \cdot B \cdot \sqrt{N}} \tag{1.4}$$

where B is the magnetic field of the trap, Q is the charge state of the ion, T_{RF} is the time required to complete the measurement and N is the number of ions measured [7]. Therefore, an increased charge state generated by the EBIT would allow for measurements on short-lived or less abundantly-produced isotopes while maintaining a high precision.

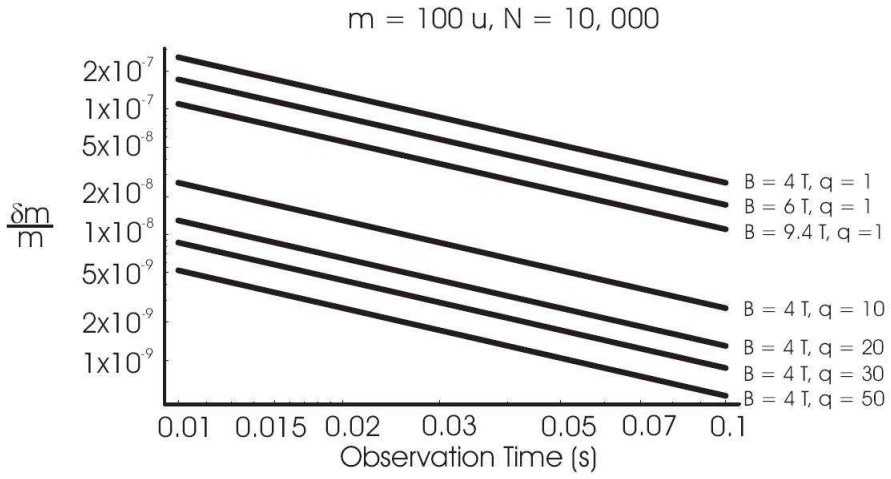

Figure 1–4: The effect of higher charge on the precision that can be achieved in the Penning trap.

The EBIT consists of a pair of superconducting Helmholtz coils (6 Tesla) with a set of 16 trapping electrodes to provide complete three-dimensional trapping [9]. An electron gun provides a current of electrons that will strip

electrons off the trapped ions. Ions are trapped in the EBIT radially by the electron beam's space charge and axially by the trap electrodes. The ions enter and exit the trap from the same point through the collector which is opposite the electron gun. The device has radial ports to allow for x-ray spectroscopy and other experiments involving the highly charged ions.

Many charge states are produced and a specific maximum charge state can be achieved by ensuring that the energy of the electron beam is slightly higher than the ionisation energy of the innermost electron to be liberated. The desired charge state can then be selected by a Wien velocity filter after the ions exit the EBIT. A Wien filter uses crossed electric and magnetic fields to selectively alter the trajectories of ions based on their charge to mass ratio. Assuming that only one ion species is present, this will allow the choice of charge states to continue along the experimental path. The EBIT has been shipped to TRIUMF and is undergoing installation and further testing at present. Figure 1-5 shows a schematic of the TITAN EBIT [8].

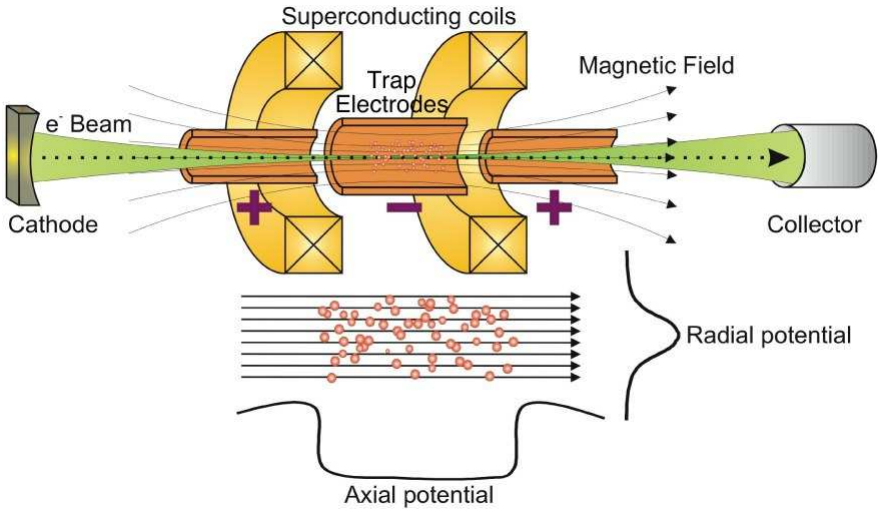

Figure 1–5: The basic principle of the TITAN EBIT.

The TITAN Penning trap will be of the hyperboloid type and will be situated in a 4 Tesla warm bore superconducting magnet [7]. Precision mass

measurements will be performed on the highly charged ions from the EBIT as described in section 1.3.

At a later stage, an additional 'Cooler' Penning trap will be added. It will be a cylindrical Penning trap and is needed as the ions will become reheated somewhat during the charge boosting stage. The ions will be trapped here for a short length of time to be cooled via collisions. The Cooler Trap is to be designed and constructed at the University of Manitoba, Canada [10].

1.3 Ion Traps

To better study aspects of atoms, it is desirable to confine them such that unwanted interactions can be excluded. One possible way to do this is to ionise the atoms and use electromagnetic elements to confine them in free space. An ion is more strongly subject to electromagnetic forces than an electrically neutral atom, but many of its other properties remain the same. For example, confining ions electromagnetically can facilitate mass measurements via the mass dependence of the Coulomb interaction Also, decay studies can be done if detectors are placed just outside the trapping region.

Though there are many types, there are only two basic kinds of ion traps, Penning and Paul. An ion can be trapped via only electric fields or with the inclusion of a magnetic field. In the case of the Penning trap, electrostatic elements are combined with a magnetic field to confine ions. Its development is credited to Hans Dehmelt in the 1960's, including the storage of electrons in a Penning trap for 5 weeks in 1968 [11]. The Paul trap uses no applied magnetic field, instead relying solely on varying electric fields. It was developed by Wolfgang Paul during the same period of time as the Penning trap [12]. In 1989 Dehmelt and Paul shared the Nobel prize together with Ramsey for their contributions to the ion trapping field and its applications [13].

1.3.1 Penning Traps

A Penning trap consists of both magnetic and electric confining fields. Using cylindrical coordinates, a magnetic field is applied along the z-axis. Ions in this field orbit about the field lines causing them to have a spiral path in the field region. Thus, they are confined radially while in the field. If an electric field is introduced to confine the ions axially, they can be trapped in 3 dimensions.

There are two basic types of electrode configurations in a Penning trap. The cylindrical trap creates a simple one dimensional potential well that is cylindrically symmetric. This relies on the magnetic field only to confine the ions radially. The ion motion is essentially circular with only a small axial component possible.

The second type of configuration is used to create a quadrupole electric field in the z direction. To approximate a true quadrupole, the electrodes are hyperbolic in shape, shown in Figure 1-6, usually with correction electrodes in place to correct for the aberrations caused by the necessity of using finite electrodes.

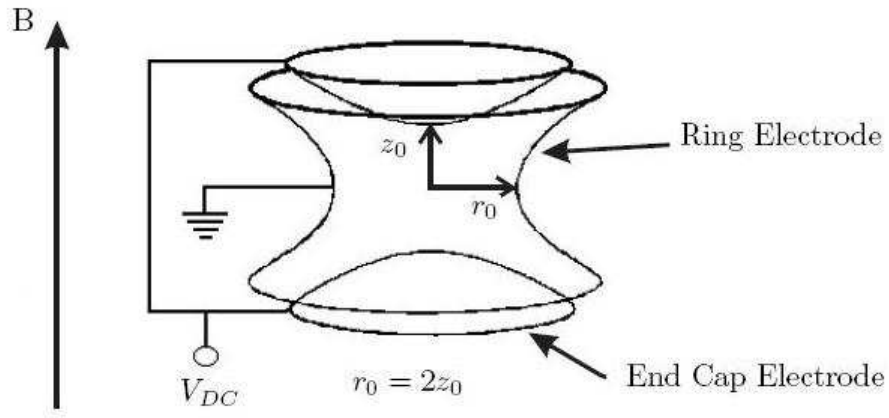

Figure 1–6: A Penning trap with hyperbolic electrode shapes.

Penning Traps for Mass Measurement

The use of Penning traps as mass spectrometers has been in place since their inception [14]. The motion of an ion in a hyperbolic Penning trap is a superposition of three separate motions shown in Figure 1-7. The magnetic field induces a slow circular motion at the magnetron frequency, ω_-. The axial motion induced by the applied electric field has a frequency, ω_z. Lastly, the interaction of the magnetic moment oriented by the magnetic field with the electric field produces a precession of the ions and leads to a fast motion at the reduced cyclotron frequency, ω_+.

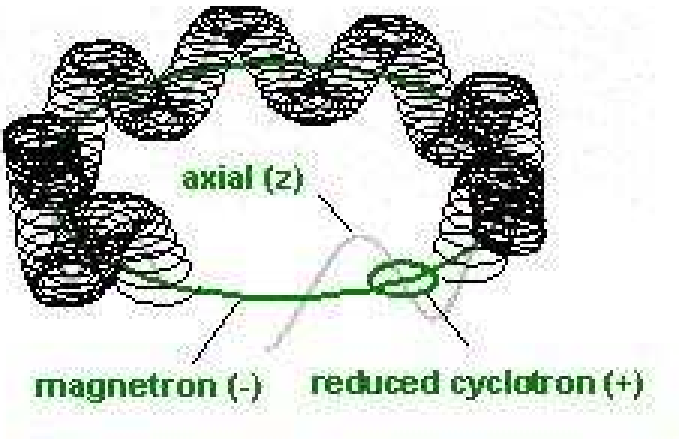

Figure 1–7: The three ion motions in a Penning trap.

The true cyclotron frequency is given by

$$\omega_c^2 = \omega_+^2 + \omega_-^2 + \omega_z^2 \tag{1.5}$$

where ω_c, is the cyclotron frequency and $\omega_+, \omega_-$and ω_z are the reduced cyclotron, magnetron and axial frequencies. The cyclotron frequency is related to the mass of the ion by

$$\omega_c = \frac{q}{m} \cdot B, \tag{1.6}$$

where q and m are the charge and mass of the ion and B is the strength of the magnetic field [15].

If an additional quadrupolar RF field is applied to the trap at the exact cyclotron frequency of the ion species, the ions will be in resonance with the field and will gain energy. This will depend on the charge to mass ratio of the ions and determination of this frequency will determine the mass of the ions for any known value of B. There are two ways to determine this frequency, a Fast Fourier Ion Cyclotron Resonance method [16] and a time of flight (TOF) measurement [17]. TITAN will use the TOF method of mass determination.

If the ions are ejected from the trap along the magnetic field lines, any additional energy they have picked up will be converted from radial energy to linear energy and the axial speed of travel of the ion will be increased. When the cyclotron frequency is reached, there is a large boost to the energy gained by the ion in the trap. A scan is carried out over a range of frequencies, determining the time from the opening of the trap to detection [17]. A representative scan is shown in figure 1-8 [18].

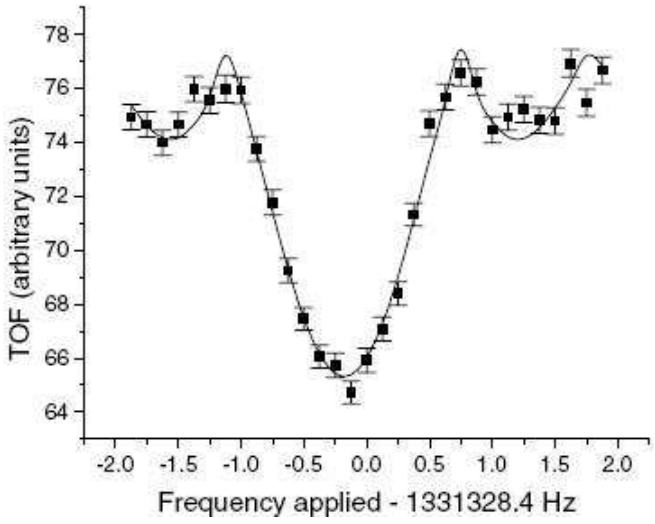

Figure 1–8: A TOF Penning trap measurement of germanium 68.

1.3.2 The Paul Trap

The Paul trap is an ion confinement device developed by Wolfgang Paul as a way to trap ions without requiring a magnetic field [12].

To trap an ion using only electric fields requires that the electric field contains a local maximum (or minimum for negatively charged ions or e^-) in 3-dimensional space. Because field lines do not cross each other, any potential that leads to a minimum in one dimension, necessarily lead to a potential maximum in at least one of the other dimensions (and vice versa for negative ions or e^-). For this reason, electrostatic fields are never sufficient and oscillating fields are used instead. Trapping is achievable with a field dependence that is of an even power in space (dipole, quadrupole, sextupole, octupole etc.). The lowest order field that can achieve ion trapping is dipolar. However, to create a dipole field to trap ions, there would have to be an extra charge in the trapping region. Thus to confine ions in an otherwise charge free region, the lowest order trapping potential to be applied is quadrupolar. An oscillating quadrupolar confining field is the basis of the Paul trap [12].

The Paul trap can have a three-dimensional trapping geometry using hyperbolically shaped electrodes and correction electrodes. In the case of the Paul trap, RF oscillating potentials are applied as well as DC potentials. In addition, the Paul trap can be implemented in a two-dimensional fashion as an ion guide or mass filter.

1.4 The Radio Frequency Quadrupole (RFQ) ion trap (or cooler)

The main subject of this thesis - the RFQ ion trap - is a gas filled linear Paul trap that will be an essential part of the TITAN system. Its purpose is to both bunch the beam, so that it is transported in bursts without losing the

majority of the ions and also to cool the beam so that the ions are transported more efficiently throughout the rest of the system.

Bunched beams are required for various reasons. First, for the type of measurements being carried out, the precision Penning trap system can only accept ions during certain times. The trap must remain closed to arrivals while the measurement takes place. Also, when the EBIT is used in conjunction with the Penning trap, ions must enter and leave the EBIT partially along the same path which would not be possible with a continuous beam.

1.4.1 Cooling

The temperature of a group of particles is a measure of how much the particles move around with respect to each other, ie. how much intrinsic extraneous energy they have. Thus, cooling the beam means literally lowering the temperature of the ions to reduce their random motion. This will allow the individual ions to pass through the experimental system all with similar velocities, which will make their transfer more efficient. One way to measure this effect is to measure the transverse emittance of a beam which indicates how much unwanted momentum the beam particles have transverse to the desired direction of the beam. This is done by measuring both the position and angular spread of the particles which can be pictured as an ellipse with the position and angle values defining the two axes. The emittance is then defined by the area of the ellipse divided by the common value Pi. More detail on the definition of this quantity can be found in section 2.4.

Similar RFQ devices have been used at several facilities. Notable examples are Isoltrap at Isolde and Jyfltrap at Igisol in Jyväskylä, Finland [19] as well as at the Canadian Penning Trap (CPT) at Argonne National Laboratory [15] in the United States. For the latter, it acts as the second stage of a 'gas catcher' system to slow down the highly energetic (MeV/nucleon) produced

ions. These RFQ beam coolers and bunchers have been used to improve the transport qualities of the ion beam. The Jyfltrap group cites a beam emittance (measure of the transversal energy spread, see chapter 2.4 of this work) of approximately 3 π-mm-mrad at an energy of 40 keV [19].

In addition to the use of the RFQ with the Penning trap system, it will be possible to send a beam to the EBIT for spectroscopy experiments on highly charged ions or back along the ISAC beam line for other experiments including laser spectroscopy. For laser spectroscopy, gating during the time that laser photons interact with the beam pulses will greatly improve the signal:noise ratio of a measurement.

CHAPTER 2
Theory

The TITAN RFQ is a specific type of Paul trap that employs a 2 dimensional structure as an ion guide along with longitudinal confinement. It will be used with a buffer gas to cool, trap and bunch ions for use in the TITAN Penning trap mass spectrometer. The device will radially confine the ions while acting as an ion guide in the axial z direction. Additional potentials will be used axially to trap and bunch the ion beam.

2.1 The RFQ: A Linear Paul Trap as a Beam Cooling Device

A Paul trap can be used in conjunction with an inert buffer gas to trap ions in a region and then use buffer gas cooling to reduce the temperature of the ions.

A three-dimensional trapping quadrupolar field has the form:

$$\vec{E} = E_o(\lambda\vec{x} + \sigma\vec{y} + \gamma\vec{z}) \tag{2.1}$$

where E_o is the overall field strength and λ, σ and γ are the components in each direction [20]. The potential in this field is then

$$\Psi = \Psi_o(\lambda x^2 + \sigma y^2 + \gamma z^2) \tag{2.2}$$

where Ψ_o is $E_o/2$.

Since the interior of the trap has no electrodes, the electric field must satisfy the Laplace equation

$$\vec{\nabla} \cdot \vec{E} = 0. \tag{2.3}$$

The simplest non-trivial solutions are then

$$\lambda = -\sigma; \tag{2.4}$$

$$\gamma = 0 \tag{2.5}$$

for a 2 dimensional trap and

$$\lambda = \sigma; \tag{2.6}$$

$$\gamma = -2\sigma \tag{2.7}$$

in 3 dimensions.

In a linear RFQ trap, the alternating fields confine in 2 dimensions and the third trapping dimension is achieved by a separate DC field. So, examining the two dimensional case yields a potential of Ψ with the form

$$\Psi = \Psi_o \lambda (x^2 - y^2). \tag{2.8}$$

A geometry that gives this form of potential would be a set of four hyperbolically shaped electrodes, with equal but opposite polarity voltages placed on the pairs. This is not practical however, as to create a true quadrupolar potential would require that the electrodes be infinite to avoid aberrations due to the edges of the electrodes. It has been found that the field near the center of the structure is quadrupolar with minimal defects close to the electrodes if circular rods are used [21] instead, provided that the radius of the rods satisfy

$$r = 1.148 r_o \tag{2.9}$$

where $2r_o$ is the spacing between two opposing rods as shown in Figure 2-1.

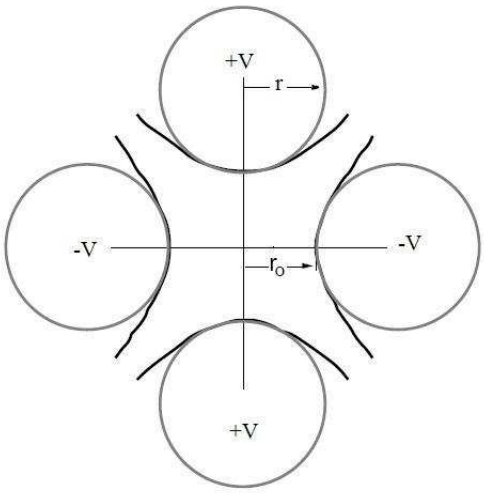

Figure 2–1: The circular rod structure approximates the quadrupolar field generated by hyperbolic electrodes provided the radius of the electrode is 1.148 times that of the radius of the opposing spacing.

For a case in which both DC and oscillating components are applied to the electrodes, the applied potential between two neighbouring rods can be written as

$$\phi_o = U - V cos(\Omega t) \tag{2.10}$$

where U is the amplitude of the DC part of the applied voltage and the alternating component is characterised by its amplitude V and frequency Ω [20]. The field potential is then

$$\Phi = \frac{\phi_o}{2r_o^2}(x^2 - y^2). \tag{2.11}$$

The equations of motion for an ion of mass m and charge Ze in the transverse directions are then

$$\begin{bmatrix} x \\ y \end{bmatrix} + \frac{Ze}{mr_o^2}(U - V cos\Omega t) \begin{bmatrix} x \\ -y \end{bmatrix} = 0, \tag{2.12}$$

which are known as the Mathieu equations for the system [20]. In order to simplify the equations, we define 3 dimensionless parameters:

$$a = a_x = -a_y = \frac{4eU}{m\Omega^2 r_o^2} \tag{2.13}$$

$$q = q_x = -q_y = \frac{2eV}{m\Omega^2 r_o^2} \tag{2.14}$$

$$\xi = \frac{\Omega t}{2}. \tag{2.15}$$

Then both equations of motion have the form

$$\frac{d^2u}{d\xi^2} + (a_u - 2q_u cos2\xi)u = 0, \tag{2.16}$$

where u is either x or y. The solutions have the form

$$u(\xi) = \alpha' e^{\mu\xi} \sum_{n=-\infty}^{\infty} C_{2n} e^{2in\xi} + \alpha'' e^{-\mu\xi} \sum_{n=-\infty}^{\infty} C_{2n} e^{-2in\xi}, \tag{2.17}$$

where α' and α" are integration constants and C_{2n} and μ are related to the values of a and q. Only certain regimes of solutions are stable depending on the value of μ. Since μ is a function of a and q, a stability region can be defined in these parameters as shown in Figure 2-2 [22].

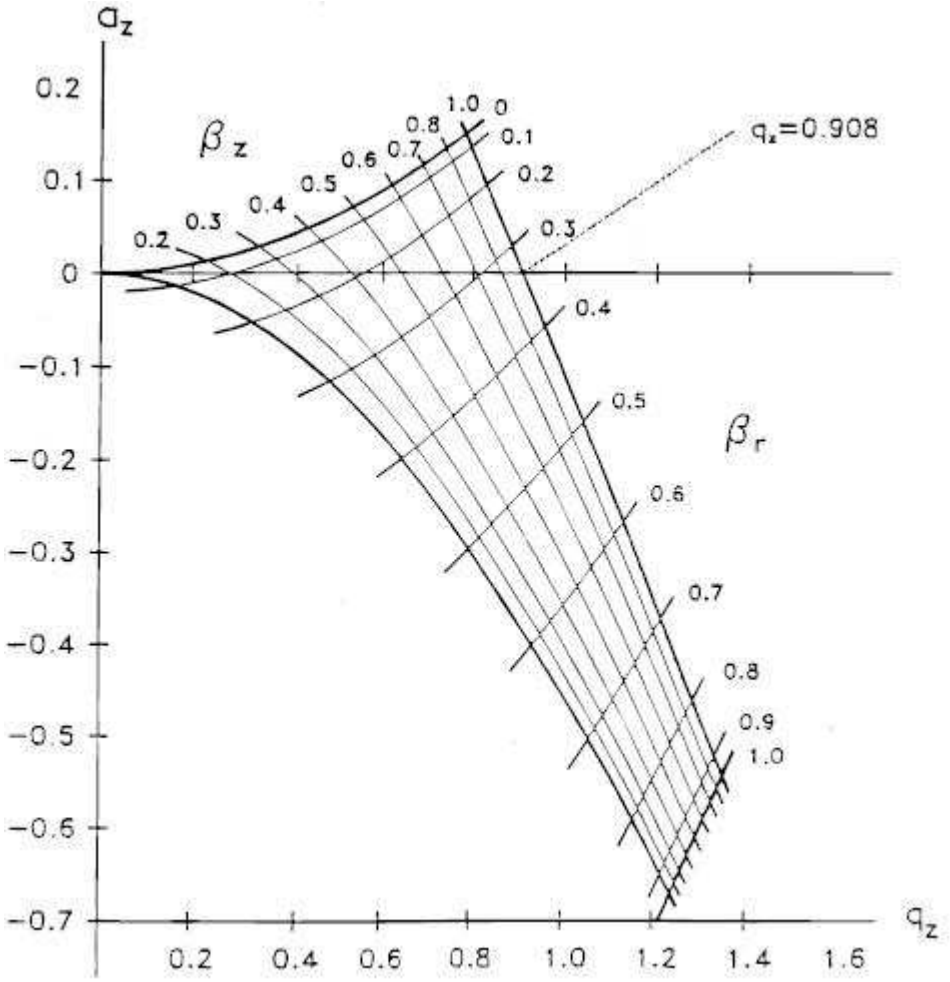

Figure 2–2: Stable trapping region for values of a and q.

The stable solutions are periodic [20] and can be written as

$$u(\xi) = A \sum_{n=-\infty}^{\infty} C_{2n} cos(2n + i\mu)\xi + B \sum_{n=-\infty}^{\infty} C_{2n} sin(2n + i\mu)\xi. \tag{2.18}$$

This shows the motions to be a superposition of periodic oscillations with frequencies given by

$$\omega_n = (2n + i\mu)\frac{\Omega}{2}, n = 0, 1, 2.... \tag{2.19}$$

The stable motion contains the lowest frequency called the macromotion and higher harmonics referred to as the micromotion. Though the motion is complicated, to first order the ions can be thought of as moving in a pseudo-potential well of depth V_{RF} [14] given by

$$V_{RF}(r) = \frac{qV}{4r_0^2}r^2. \tag{2.20}$$

In an RFQ ion guide acting as a mass filter it is advantageous to have no DC component to the radial field, thus setting a=0 [12]. The motion of the ions in the device is therefore completely dependent on the q value, which contains the dimensions of the trap and the applied RF amplitude. The only ion-dependent parameter involved is the mass. Thus the voltage can be set to have stable trajectories for ions with certain mass-to-charge ratios thereby acting as a high pass mass filter with finite resolving power for a mixed beam of different elements or isotopes [12].

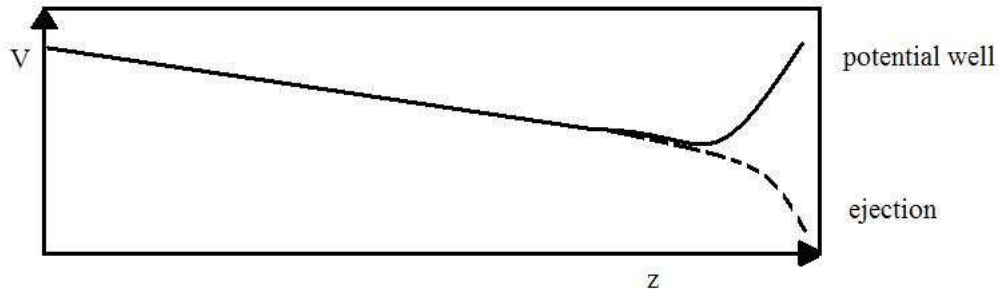

Figure 2–3: The applied linear DC field leads to bunching via switching of the potential from trapping to ejection mode.

Bunching and cooling can then be achieved by segmenting the rod electrodes to provide a DC gradient along the axis as well as a potential well for trapping. The trapped ions can then be cooled by adding an inert buffer gas. The cooled and trapped ions that have accumulated in the potential well can

then be extracted out of the structure by switching the voltages on the end electrodes shown in Figure 2-3.

2.2 Square Wave Drive Voltages

The previous discussion centered around a sinusoidal applied potential to radially confine the ions. TITAN's RFQ uses a square wave pulse with two opposite polarity states with amplitude ±V. A square wave linear Paul trap was first used by J. Richards to drive a trap at an amplitude of 80 V and frequencies up to 1 MHz [23] but the technology to handle the energy dissipation in switching high capacitive loads such as a longer RFQ at higher amplitudes has come about only recently.

The different RF generation has two main effects. First, the use of a square wave over a large frequency range will make it possible to reach stable q values inside the device for a wide range of ion species and isotopes. This is in contrast to a sine wave which is generated by an RF amplifier and the two phases separated using ferrite cores that have small bandwidths due to heating effects [24]. Second, the pseudo-potential generated by a square wave will be deeper than that of a sine wave for the same applied amplitude, meaning that fewer ions will get lost [25]. As has been discussed previously, the efficiency of the system is a crucial parameter.

For square waves, we define a function S_δ with δ such that

$$S_{0.5} = \begin{array}{ll} 1 & 0 \leq t \leq T_{1/2} \\ -1 & T_{1/2} \leq t \leq T \end{array}, \tag{2.21}$$

where T and $T_{1/2}$ are the period and half period of the oscillating motion and t is a time within that period. The equations of motion then become:

$$\begin{bmatrix} x \\ y \end{bmatrix} + \frac{e}{mr_o^2} 2S_{0.5}V \begin{bmatrix} x \\ -y \end{bmatrix} = 0, \tag{2.22}$$

and the q value is now given by

$$q = \frac{4eV}{m\Omega^2 r_o^2}. \tag{2.23}$$

A new quantity h is defined by

$$h = \sqrt{2q}, \tag{2.24}$$

to give the canonical form of the Mathieu equations as:

$$\frac{d^2u}{d\xi^2} + h^2u = 0 \qquad 0 < \xi \leq \frac{\pi}{2}, \tag{2.25}$$

$$\frac{d^2u}{d\xi^2} - h^2u = 0 \qquad \frac{\pi}{2} \leq \xi \leq \pi, \tag{2.26}$$

These have solutions which are a subset of a class of equations known as Hill equations. The stable solutions have the form

$$u(t) = \Re\left[A \sum_{n=-\infty}^{\infty} C_n exp[i(n\omega + \omega_s)t]\right]. \tag{2.27}$$

As in the sinusoidal case, these form a Fourier series of oscillating frequencies

$$\omega_n = |n\omega + \omega_s| \quad n = 0, \pm 1, \pm 2... \tag{2.28}$$

with the lowest frequency describing a slow harmonic macromotion and the higher frequencies giving rise to micromotion perturbations.

The TITAN RFQ has a r_o of 10 mm giving a q value for the system of

$$q_{TITAN} = \frac{4eV}{m\Omega^2 r_o^2} = \frac{400eV}{m\Omega^2} \tag{2.29}$$

for amplitudes V up to 1000 V_{pp} and masses m above 1.33x10^{-26} kg (8 amu) [26] .

2.3 Buffer Gas Cooling

The cooling of the ions involves slowing or stopping them so that the random motion is stilled and purely longitudinal motion can be introduced. In practice there is always some transverse momentum introduced due to space charge effects and interactions with the buffer gas. Even in principle one cannot reach absolute zero. The lowest temperature that can be reached is determined by a combination of the number of ions (as their interactions with each other will have an effect), the temperature of the gas and the potential depth of the trap. The gas pressure affects how long it takes for the ions to reach that state, making the amount of time the ions are collected and cooled for a given pressure important.

The cooling of the ions is accomplished via an inert buffer gas introduced to the system. The ions will undergo collisions with the gas, lose kinetic energy and slow down. It is important that the gas be inert and relatively pure (at least 99.998% purity level) in order to avoid chemical reactions with the ions. In addition, during collisions with the gas atoms there is a danger of charge exchange, which would cause the ions to be lost. To decrease the probability of this happening, we must use a gas with a high ionisation potential. The requirements of inertness and high ionisation potential make helium the best choice (ionisation potential: 24.58 eV) followed by neon(ionisation potential: 21.56 eV) and argon(ionisation potential: 15.76 eV).

The other important consideration in choosing a gas is the stopping potential. This is loosely a measure of how far the ions have to go in the gas before they are stopped or more rigorously until their forward momentum is negligible compared to their thermal motion. It is dependent on the density of the gas (pressure) and the relative masses of the gas and ions.

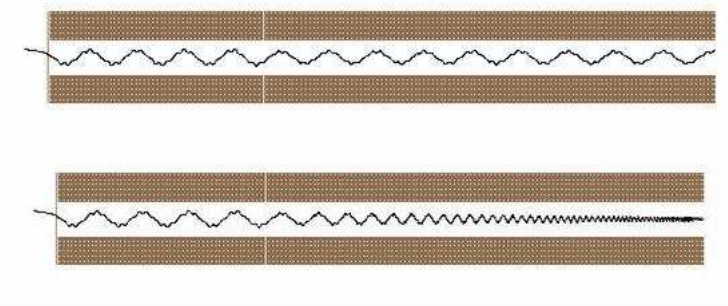

Figure 2–4: Simulated ion motion without and with buffer gas in the RFQ ion guide (length = 700 mm)

Figure 2-4 shows a simulation of a long RFQ structure and the damping effects of buffer gas on ion motion in an RFQ ion guide. The oscillatory motion can be seen in the first case and the reduction of the amplitude of the motion is shown in the second case. This example is for cesium ions and He buffer gas at a pressure of 2.5 Pa. These are close to the parameters that will be used in the TITAN RFQ.

2.3.1 Ion Mobility

If the ions are diffuse spatially, their Coulomb interactions can be ignored and their behaviour in the gas can be treated as a combination of the drag effect of the applied DC field (drift) and the scattering (diffusion) of the ions with the gas atoms. Turning this around, the drift velocity of a cloud of ions through a gas is related to the strength of the applied field and a quantity called the mobility, K [27]

$$\vec{v_d} = K\vec{E} \tag{2.30}$$

where $\vec{v_d}$ is the drift velocity of the ions through the gas and $\vec{E}$ is the electric field present.

This relation is valid for relatively weak electric fields and near thermal equilibrium between the ions and gas. The mobility of the ions through the gas depends on the properties of the ions and the gas and is dependent on the temperature of the system and the pressure of the gas. It is usually stated in reference to a standard mobility at 0° Celsius (273.15 Kelvin) and standard atmospheric pressure.

$$K = \frac{T}{273.15}\frac{760}{P}K_o, \tag{2.31}$$

where T is in Kelvin and the pressure P is in Torr. K_o, the value of which is dependent on the type of gas, can be found in data tables and is derived from experiments [28].

In this model of ion motion, the buffer gas therefore has the effect of introducing a drag force to counteract the motion of the ions through the weak electric field. This force is proportional to the drag velocity of the ions,

$$F_d = \frac{q}{K}v_d. \tag{2.32}$$

The deceleration effect is then given by

$$ma = \frac{q}{K}\dot{z}, \tag{2.33}$$

where q is the charge of the ion and $\dot{z}$ is the velocity of the ion through the gas. The velocity of the ions as a function of time through the gas is given by

$$v(t) = v_d e^{-\frac{q}{Km}t}, \tag{2.34}$$

which when combined with tabulated data of the mobility [28] gives an estimate of how long ions will take to cool to a certain temperature in the buffer gas.

2.3.2 RF Heating

While the ions are being confined and cooled, the RF does have a small heating effect. The oscillatory nature of the applied field adds energy to the ions as they sit inside the trap. In the interior of the structure, the cooling effect of the gas balances the heating of the RF. However, when the ions are exiting the trap, if there is significant RF leakage outside the confines of the RFQ structure, a differential pumping section is entered and the gas pressure will be significantly lower. This will decrease the residual cooling effects of the gas and the ions will be in a region of oscillating field with little or no damping of the induced motion. This will result in the decoherence of the beam [29].

This effect is compounded by space charge effects of the ion cloud. When the ions are confined, the Coulomb repulsion they feel is somewhat negated by the cooling and the RF and DC confinement. However, when the ions leave the trapping region, the confining force is reduced. The Coulomb repulsion between the ions takes over and the ion cloud spreads out.

Both of these effects combine to limit the lower bound of the temperature that can be achieved with the device. The temperature the ions have when they have fully exited the RFQ area will be slightly higher than the temperature reached inside the trap.

2.4 Emittance

Phase space is the six-dimensional space a particle inhabits consisting of its position and momentum. A phase space diagram in each of the three dimensions consists of the particle's position and momentum in this direction. A collection of particles can be described by the shape of the projection of the collection into phase space. The distribution of the positions and velocities gives an indication of the overall behavior of the beam.

The emittance of an ion beam is related to the envelope of its projection in phase space. Every ion in the distribution has a position and velocity in all three orthogonal directions. The overall pattern of these quantities will define the emittance in each direction. A beam of ions traveling along the z axis has emittances in both transverse planes as well as longitudinally. In a particular direction x for example, the phase space diagram of simple harmonic motion would look like Figure 2-5.

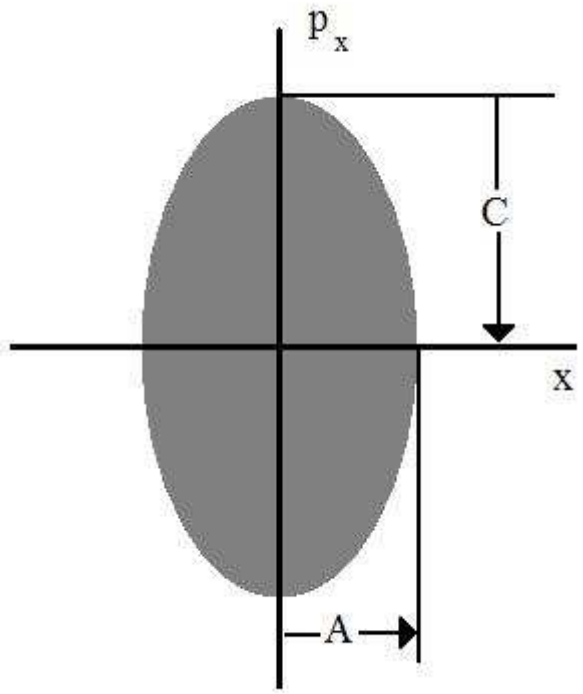

Figure 2–5: Phase space diagram of particles undergoing simple harmonic motion

Liouville's theorem states:

For a cloud of moving particles, the particle density $\rho(x, p_x, y, p_y, z, p_z)$ in phase space is invariable [30]

which is valid when the forces on the particles are conservative and all forces can be written as the gradient of a potential. This is true of an ion beam

transported using optical elements assuming that the ion-ion interactions are minimal. The emittance is a characterisation of this phase space area. It is possible through optical elements to bring the beam to a focus, confining the position of the beam. However this will increase the momentum distribution such that the area of the ellipse remains the same. Thus, the area of the ellipse is a basic property of the ion collection and the emittance is defined by

$$\epsilon = \frac{Area}{\pi} = AC \tag{2.35}$$

where A and C are the semi-minor and semi-major axes respectively. The emittance is usually reported as the area in units of $\pi - mm - mrad$ to indicate the inclusion of the factor of π.

The longitudinal emittance of a beam is related to the longitudinal energy spread that the ions have from their source. This will determine the time spread that ions starting at the same time will arrive at a specific location down the beam line, with the more energetic ions arriving first.

The transverse emittance of the beam reflects how much transverse velocity the ions have. If no other forces are present, this indicates how much the beam will spread out transversely as the ions are transmitted. In this way, the transverse emittance is therefore related to the divergence of the beam.

$$\epsilon_x = x \cdot mv_x \tag{2.36}$$

$$\epsilon_x = x \cdot mv_z \cdot tan(x') \tag{2.37}$$

Using a small angle approximation, the emittance can then be written as

$$\epsilon_x = x \cdot mv_z \cdot x', \tag{2.38}$$

where x' is the angle between the ion trajectory and the z axis shown in Figure 2-6. Since the energy of a non-relativistic particle is simply

$$E = \frac{1}{2}mv^2 \tag{2.39}$$

and since the particles have velocities satisfying $v_z >> v_x$, this can then be expressed as

$$\epsilon_x = x \cdot x'\sqrt{2mE} \tag{2.40}$$

which then permits comparison of emittances at different energies.

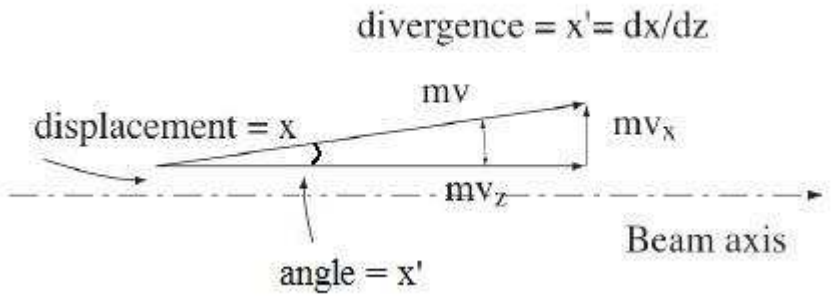

Figure 2–6: Divergence of an ion beam

The parameters used to describe emittance can also be used to describe the acceptance of a device in a beam line. For an ion beam that is wider than the optical element, the outermost ions will not enter and will be lost. Also a beam that is narrow but too divergent will result in ions striking the edges of the electrode and be lost. The acceptance of a beam element is defined by the 2D phase space plot of ions that can be transmitted through the element.

The maximum transmission occurs when the emittance of the beam and the acceptance of the system are matched. Even if the scalar emittance number is the same, the orientation of the ellipse and the existence of tails may be different which would introduce losses. Therefore it is important to know not

just the area of the ellipse but also its x and x' extents as well as the rotation angle r_{12} which describes the angle between the semi major axis of the ellipse and the horizontal axis. These three quantities, pictured in Figure 2-7, will completely characterise the ellipse and studies of emittance and acceptance can be performed.

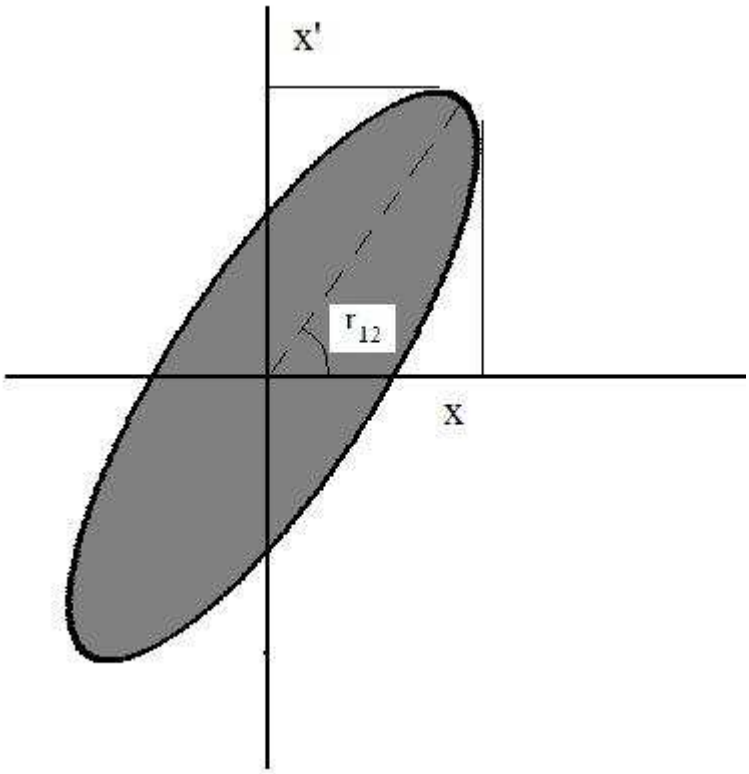

Figure 2–7: A rotated ellipse showing the three parameters

In an RFQ cooler and buncher, the collisions of the ions with the buffer gas are not elastic, making the cooling process non-conservative. Thus, Liouville's theorem is not applicable. The device can therefore cool the beam and reduce its emittance.

The emittance reduction and the bunching capabilities of the RFQ will permit the incoming ISAC beam to be used for discrete transport and high

precision experiments such as TITAN's planned mass measurements. In addition, the extraction optics after the RFQ (discussed in Section 3.4) will allow for the exiting beam to be at a different energy than the incoming ISAC beam. The emittance of the Low Energy Beam line (LEBT) at ISAC is approximately 11 π-mm-mrad [1] at an incoming energy of 40 keV and the expected emittance of the beam exiting the RFQ is 5-10 π-mm-mrad at an energy of 2.5 keV (see section 4.1 or [24]). Extrapolating the expected results from the RFQ to the higher energy via equation 2.39 to make a direct comparison shows that at an energy of 40 keV, the cooled beam would have an emittance of 1.25-2.5 π-mm-mrad giving a reduction of over 75%.

CHAPTER 3
Experimental Setup

The testing of the RFQ buncher operation was done at an off-line test stand. It was capable of floating the RFQ electrodes and ion source up to a potential of 30kV above ground to simulate the operation of the device when used in conjunction with the ISAC facility. The test stand and ion optics were chiefly designed by Mathew Smith based on his simulations [24]. The test stand consists of three portions; the ion source and injection optics, the RFQ itself and the extraction optics and ion detection. The first section contains a surface ion source and electrostatic elements to bring the ion beam to the RFQ. The RFQ tank contains the RFQ itself and all associated feedthroughs. The exit cross contains the same electrostatic elements that will be used in the final TITAN beam line. The test stand will therefore allow us to test the behaviour of the RFQ as well as the injection and extraction optics similar to the planned ISAC beam.

Figure 3-1 shows a schematic of the basic components of the test stand, which consists of the ion source/entrance cross, the RFQ tank and the exit cross [24]. The voltage bias of the main components is shown with the RFQ at V with respect to ground, and the ion source and extraction drift tube at values of V + ΔV_1 and V - ΔV_2 respectively.

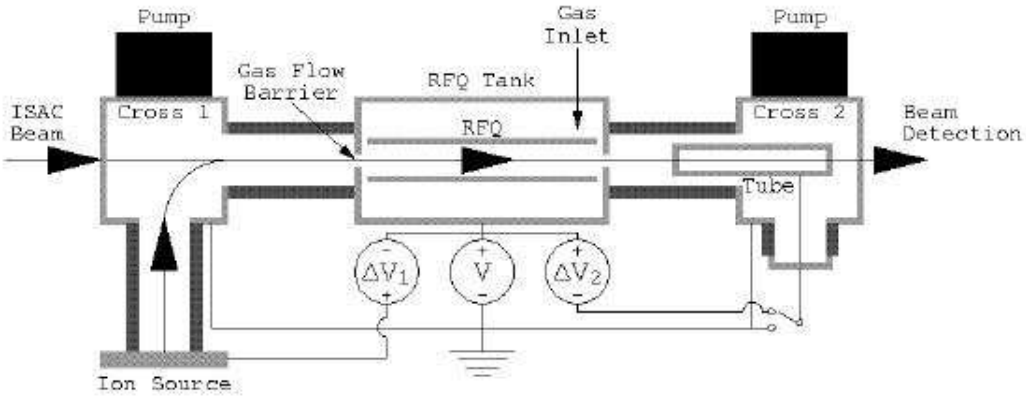

Figure 3–1: Schematic of the RFQ test stand.

The RFQ and the ion source are held at high voltage, and their associated power supplies are housed in an electrical rack which is floated to the bias potential. The rack, shown in figure 3-2 sits in a cage above a transformer. The voltages for all the electrodes in the RFQ are supplied from this rack.

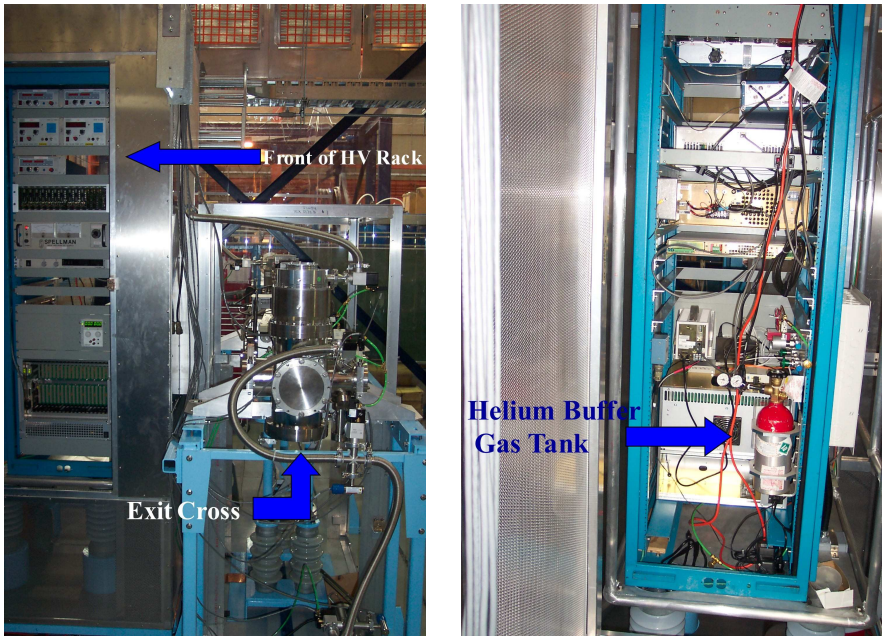

Figure 3–2: A photograph of the high voltage rack for the RFQ

A photograph of the test stand is shown in Figure 3-3, without the RFQ electronics that would normally be housed on the lid of the RFQ tank.

Two turbo pumps (one 1000 l/s and one 500 l/s) mounted on both the main injection and extraction crosses provide a vacuum of $7x10^{-3}$ Pa when the pressure inside the RFQ tank is 1.3 Pa. The gas is fed into the tank via a 1/4 inch aluminum tube attached to a small helium tank housed in the high voltage rack. Two on/off valves and a mass flow controller dictate the flow of gas into the system. For the tests presented in this work, a larger gas tank was used externally to the HV rack and fed into the existing gas line in the HV rack via PVC tubing.

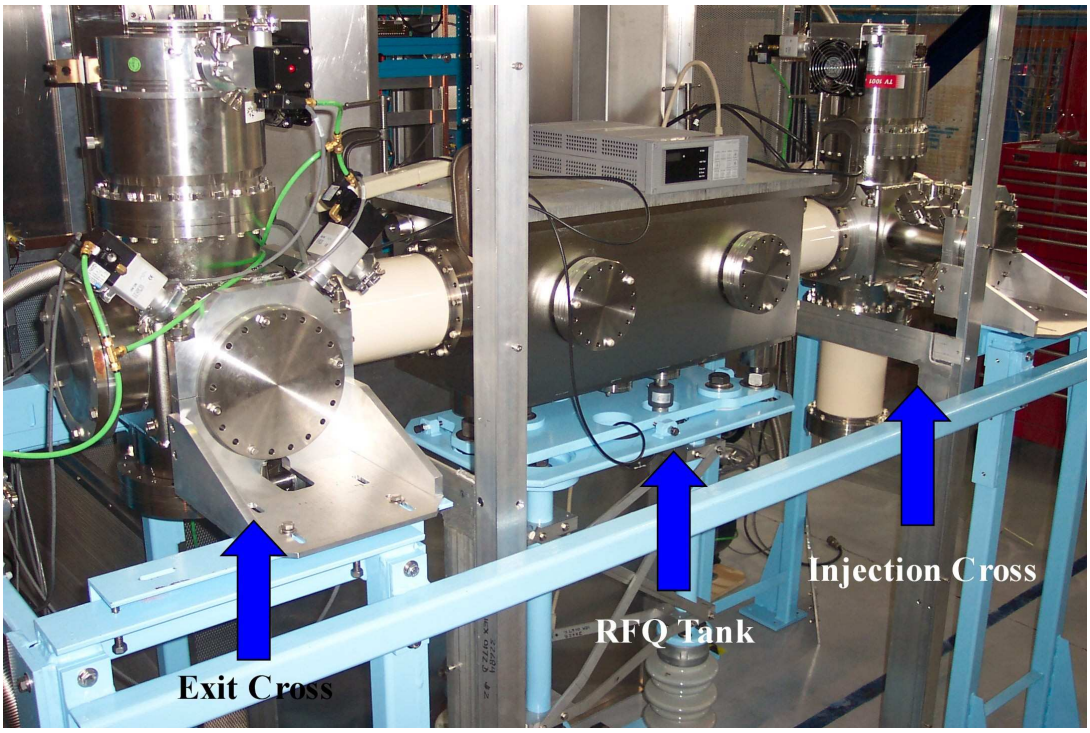

Figure 3–3: A photograph of the RFQ test stand showing the ion source cross on the right hand side, the RFQ box and the exit cross

3.1 Ion Source and Injection Optics

3.1.1 Ion Source

The RFQ is designed to be floated to a bias potential to match the incoming energy of the ISAC beam. This allows the device to stop beams of various energies in a low pressure buffer gas as the bias can be adjusted with respect to the incoming beam. To conduct the testing of the RFQ, we also floated the ion source to give the incoming ions just a few eV more energy than the RFQ potential. This will simulate the true injection of the ISAC beam.

The ion source used to generate our test ions for the system is a surface ionisation cesium 133 source from Heat Wave Labs pictured in Figure 3-4 [31]. The source consists of packed cesium in a molybdenum casing with a filament running inside. The two ends of the filament are connected via posts extending from the bottom of the source and ions are generated by heating the filament via an applied current of 3-4 A. The source floats on high voltage using the same supply that provides the bias for the RFQ structure. The ions are emitted thermally and the source is operated with a temperature of 2400 K. The cesium ions are then accelerated toward an anode and through a grounded cone and drift tube to emerge with the full bias energy corresponding to the applied potential (between 5 and 30 keV for these tests).

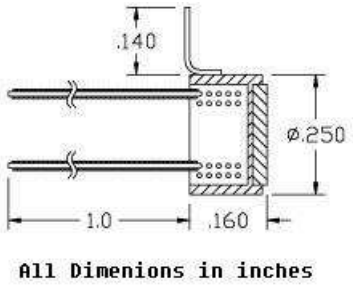

Figure 3–4: Schematic of the ^{133}Cs ion source

3.1.2 Ion Transport

The ions are transported through the RFQ test setup by a system of electrostatic elements. This will simulate the energy and emittance properties of the expected ISAC beam, which is essential in understanding the real working conditions of the device. A schematic of the ion source and injection optics is shown in figure 3-5 [24].

After leaving the ion source, the ions go through a set of quadrupoles to shape the beam. These consist of 3 cylindrical electrodes cut axially to form 4 quadrants. For each of the electrode sections, a specific voltage is applied, positive on two of the oppositely facing pieces and negative on the other two. This is reversed on the middle of the three sections and then the third is the same as the first. In order to get a symmetric overall focusing effect, it is usual to have the middle of the three sections be twice as long as the other two. In our case, due to practical space limitations, it was decided that we would instead have the voltages on the middle section be approximately twice as large, while keeping the length the same as the other two sections. These electrodes are known as Q1 for the first and third sections and Q2 for the second section.

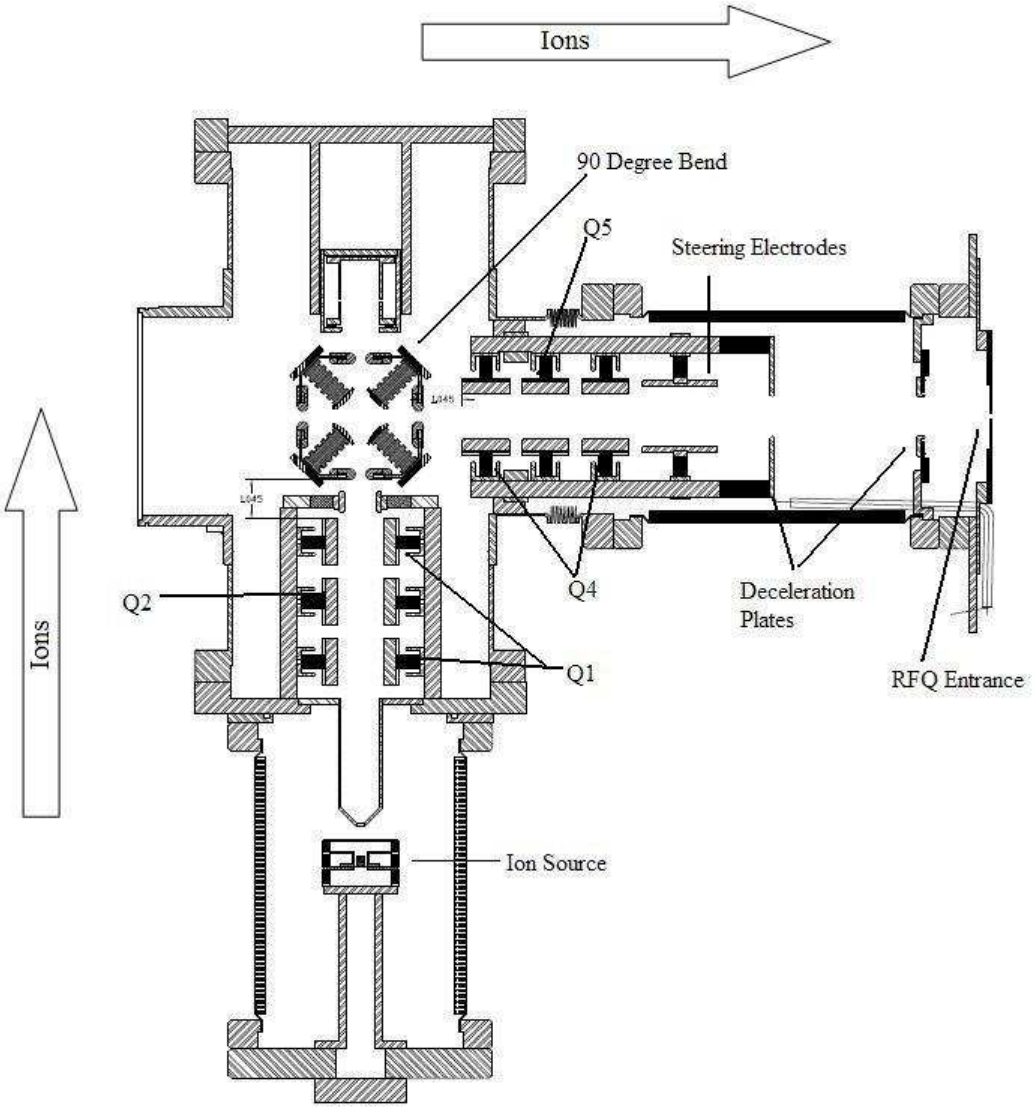

Figure 3–5: Schematic of the ion source and injection optics.

The ion source sits at right angles to the RFQ beam line in the test stand. This was initially designed to allow the stable ion source to be accessible when the device is attached to the ISAC beamline. The design for final installation

was later revised to not include this bend. The test stand, however, did require a way to bend the beam around a corner was needed. Again, space constraints played a role in the design of such a device, as well as the necessity to determine how well the 90 degree bender would work on higher energy beams. The four way bender design is set up so that a beam entering from one direction can exit in one of 3 different directions depending on the strength and polarity of the voltage applied to the plates and is shown in Figure 3-6. The four hyperbolic segment shaped electrodes provide a quadrupolar field so that the ions can be bent 90 degrees. The voltages needed to create a strong enough field to change the ion trajectory by 90 degrees are substantial. With the ions having been accelerated to an energy of 30 keV, the voltages required to bend the beam are ±26 500 V, applied in pairs such that opposing electrodes carry the same polarity.

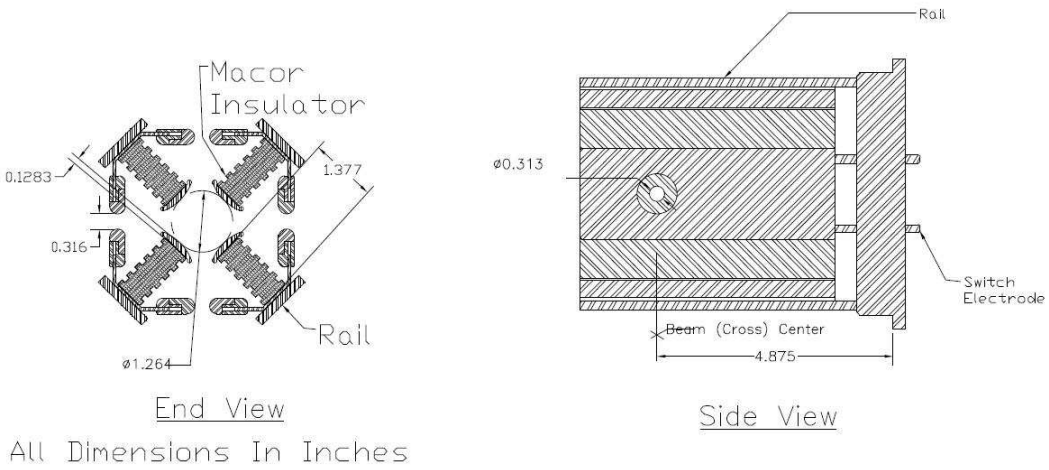

Figure 3–6: Schematic of the 90 degree bender. The ions enter and exit through holes at 45 degrees to the electrodes.

After the ions have been bent around the corner, they go through another quadrupole triplet and a steerer. The steerer is a cylindrical electrode cut in

four pieces so that voltage can be supplied to each piece independently. This is used for subtle corrections to the direction of the beam into the RFQ. The last two elements of the injection into the RFQ are a set of two deceleration plates. The beam has been accelerated to a high energy to simulate the incoming ISAC beam, so the ions after the steerer have an energy of 5-30 keV corresponding to the potential.. The RFQ is floated close to this same potential, so that the energy of the ions inside the RFQ is only tens of eV. This creates a deceleration of the ions as they enter the RFQ. When a beam of ions is decelerated, the ions tend to spread out transversally. The two deceleration plates exist to give a more gradual transition and to create a field gradient such that the beam envelope does not diverge rapidly. The deceleration optics are shown in Figure 3-7 with the additional implementation of a metal tube between the two plates. This tube is held at the same potential as Decel Plate 1 and prevents the charging up of the insulating vacuum vessel between the high voltage of the RFQ tank and the bender cross at ground from stray ions.

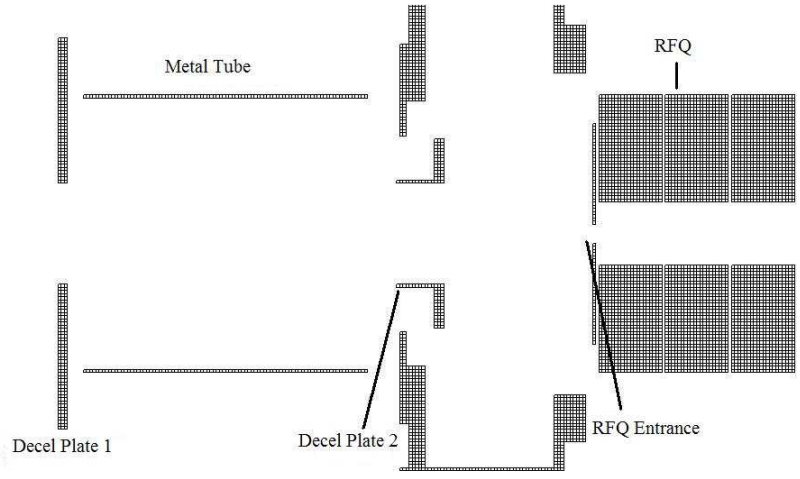

Figure 3–7: The deceleration part of the injection optics into the RFQ.

Since the RFQ is being floated at high voltage, the test ion source must be operated at a slightly higher potential than the system bias. The ion source

power supply is therefore connected to an additional voltage source. The local ground of the additional source is the HV bias and its output is up to 100 Volts above this base. The ion source supply then uses this output as its ground, thereby giving the ions just enough energy to enter the RFQ box. The relative biasing of the various components is shown in Table 3-1.

Ion Source	Entrance Cross	RFQ	Extraction Cross
30 100 V	0 V	30 000 V	0 V

Table 3–1: Biasing of the main components of the test stand.

3.2 RFQ

The RFQ electrode structure hangs suspended from the lid of the tank as shown in the photograph in Figure 3-8. The RF and DC potentials are supplied from feedthroughs on the lid as well as the gas inlet. The device will be able to cool ions and to trap them at either end of the structure for use of the cooled ions in the TITAN system or in other experiments.

The RFQ structure itself is 700 mm in length and consists of four sets of 24 U-shaped electrodes held in place by long alumina silicate holders. The middle 11 electrodes are the same length (40 mm) to provide both a uniform DC gradient as well as allowing for possible other field configurations for other applications. Six electrodes on either end are the same shape, but are shorter in length (20 mm) to give a better-defined trapping region for extraction at both ends of the RFQ. On the main extraction end of the device, the last electrode is 9mm long. There is a 0.5 mm spacing between each electrode. The holders, which also act as insulators, are attached to a frame consisting of 3 square supports at the ends and middle of the RFQ structure. This frame is then attached to the lid of the RFQ vacuum vessel.

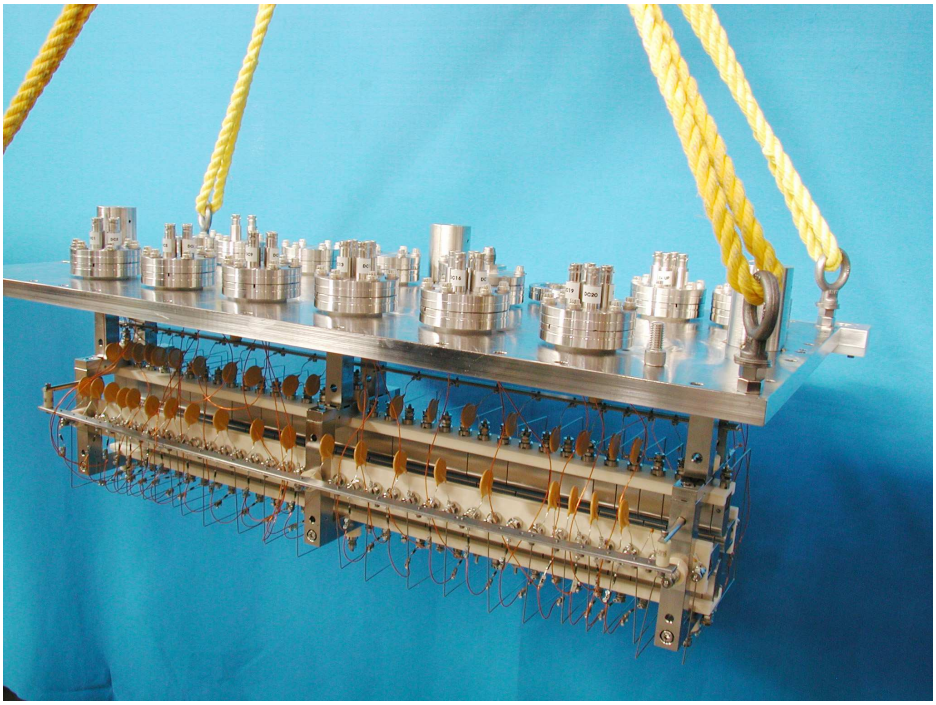

Figure 3–8: Photograph of the RFQ structure attached to the lid of the RFQ chamber

The structure can be seen in Figure 3-9 in both a side and end view [24]. The rectangular box vacuum chamber has small apertures at either end which act as gas barriers to reduce the buffer gas leakage to the rest of the vacuum system. The entire system is mounted horizontally on the test stand and will be vertical in the final TITAN setup. The alignment of the RFQ structure is done first relative to the lid and then the box. The box and apertures are then aligned to the beam line.

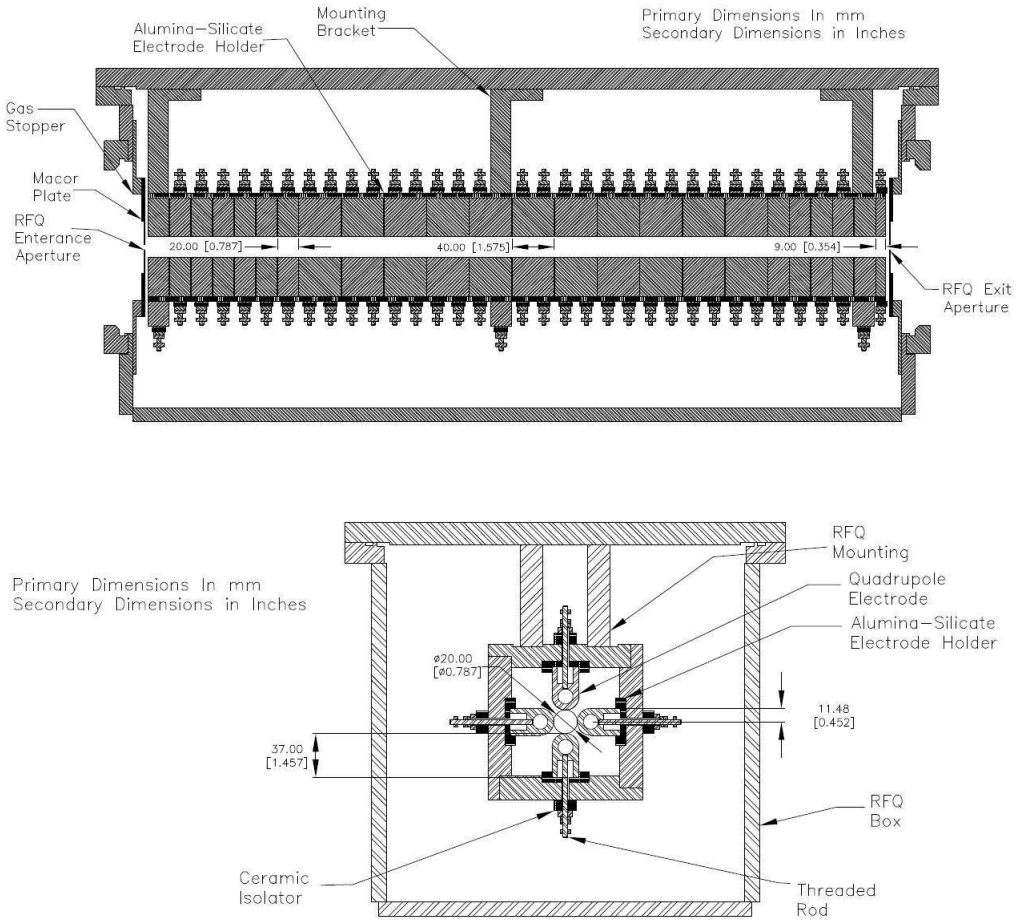

Figure 3–9: Mechanical drawing of the RFQ.

The RF potential is applied to two bus bars running along side the rod structure. Each electrode of the RFQ is fed by an independent DC power supply coupled with the RF via an RC circuit with resistor (10 MΩ) and capacitor (5.6 nF). Because the end trapping electrodes have a switching DC potential as well as the RF, a different resistance value is used for those couplings (220 pF) [26]. The coupling scheme of the RF and DC potentials is shown in Figure 3-10.

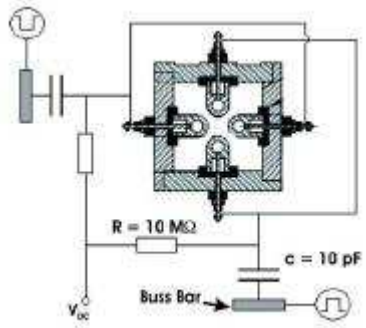

Figure 3–10: Axial view of the RFQ; coupling of the DC and RF onto the electrodes

3.3 The Driver

The RFQ is driven using a system of MOSFETs (Metal-Oxide-Semiconductor Field-Effect Transistor) in a 'push-pull' configuration to generate a square wave RF potential. The design is based on switchers developed at TRIUMF for the MuLan experiment at PSI (Paul Scherrer Institute) which is a muon lifetime experiment using similar switching techniques to drive a 25 kV, 75 kHz kicker [32].

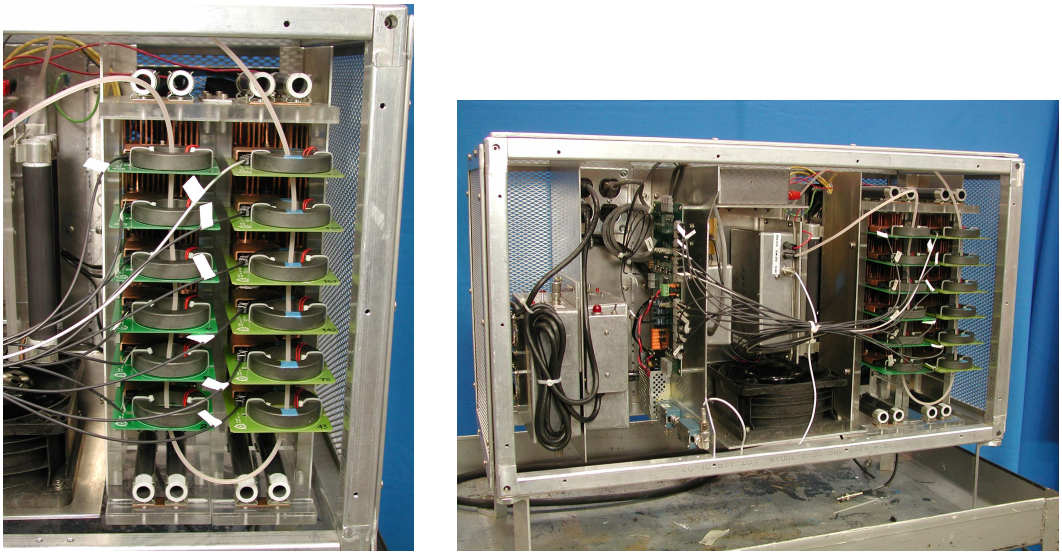

Figure 3–11: Photographs of the MOSFET driver stacks (left) and the driver housing with control board and stacks (right)

Each MOSFET can switch up to 1000 V across it. To switch higher voltages, the modules are linked together into two stacks, one stack for each phase. The stacks, shown in Figure 3-11, consist of 12 1 keV cards, 6 (3 up, 3 down) for each phase of the RF. Each card, shown in Figure 3-12 has a fast switching power MOSFET from Directed Energy Inc [33]. They have a maximum voltage rating of $V_{DS} = 1000$ V and a peak current rating of 12 A.

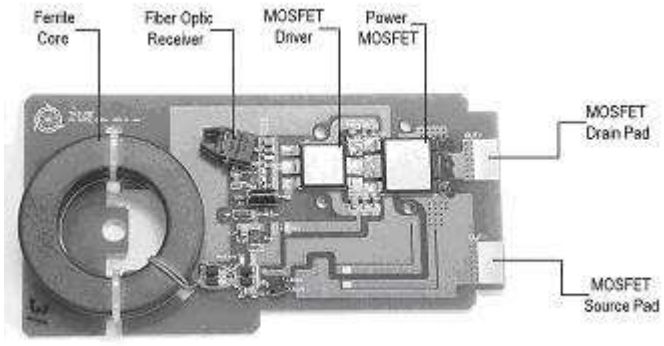

Figure 3–12: Photograph of a 1 keV FET module

Because we are switching at high rates (0.2-0.8 GHz), the power required for switching means that we cannot switch the full 1 keV across each board. By stacking them, the power available allows for switching of 400 V up to 1 GHz. This is planned to be expanded up to 600 V at a rate of 3 GHz. The boards are powered by magnetically coupling them to the 5 V power supply using ferrite cores. The basic circuit diagram is shown in Figure 3-13.

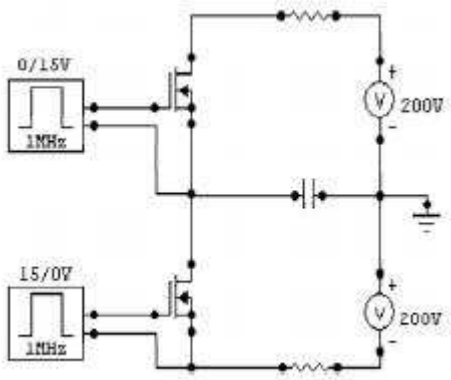

Figure 3–13: Schematic of the switching circuit

The control board consists primarily of the pulse controller board. This board has two input signals, an optical trigger for the power supply driver and a TTL signal for the FET switching trigger. These are set by a master frequency trigger in a VME crate. The power supply trigger optimises the current pulse that drives the FET boards. A schematic of the signal path is shown in figure 3-14. The TTL signal is 'copied' by the trigger board and inverted so that one copy triggers the pull up stack and one copy triggers the pull down stack.

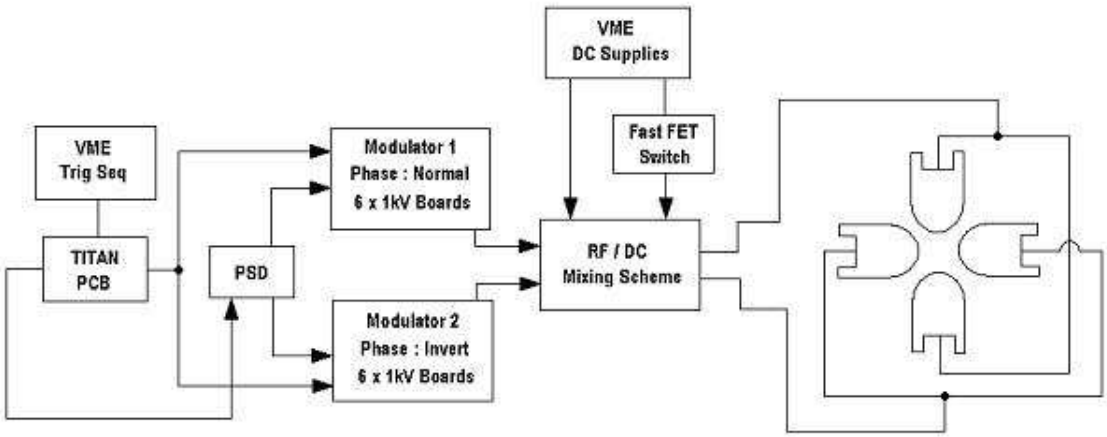

Figure 3–14: The trigger schematic for the FET driver boards.

The RF was measured at several amplitudes and frequencies to test the response of the electrodes. The signal from two of the electrodes close to the end of the RFQ were split off to electrical feedthroughs to the outside of the RFQ box so that the in situ response of the electrodes could be measured. The response of both phases at an amplitude of 600 V at 750 kHz is shown in figure 3-15 [34]. The two electrodes measured are at the same longitudinal location but are of opposite phases. The capacitive effects of the system setup on the rise and fall times was examined. The measured waveform had a rise time of 123 ns and a fall time of 118 ns [34] which are within the tolerated 125 ns [26].

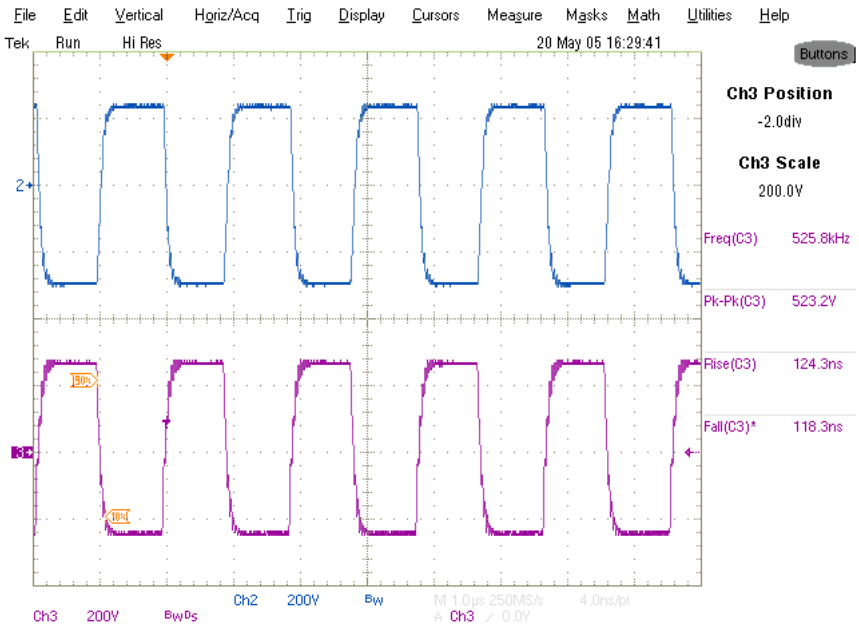

Figure 3–15: Both phases of the RF as measured directly from the electrodes.

3.4 Extraction Optics and Ion Detection

3.4.1 Extraction Optics

After the RFQ, the ions pass through the extraction optics section. This consists of a steerer, an Einzel lens and the long drift tube for energy selection. The Einzel lens is a set of 2 plates (Acel1 and Acel2) separated by a short drift tube (DT1) and focuses the beam to traverse the long drift tube. After the lens, the final element in the test stand and in the RFQ portion of the future TITAN beam line is an energy selecting drift tube. Several elements of the extraction optics are photographed in figure 3-16 while a schematic of the whole extraction optics section is shown in figure 3-17 [24].

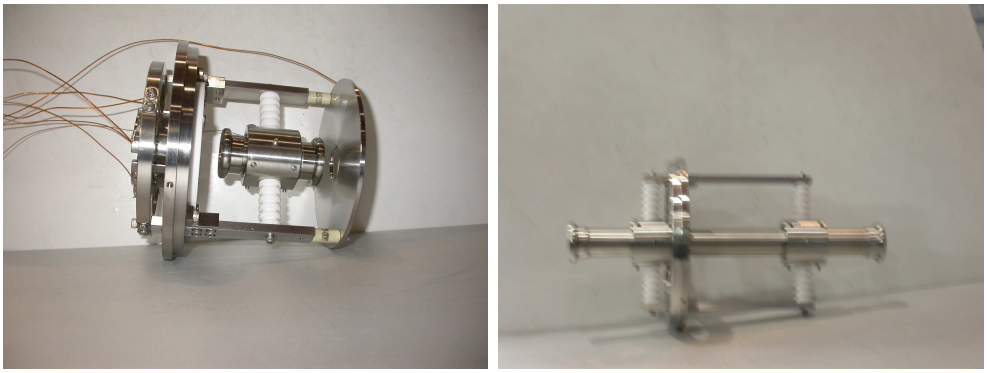

Figure 3–16: The extraction optics of the RFQ consisting of an Einzel lens/acceleration plate assembly and the energy selection tube.

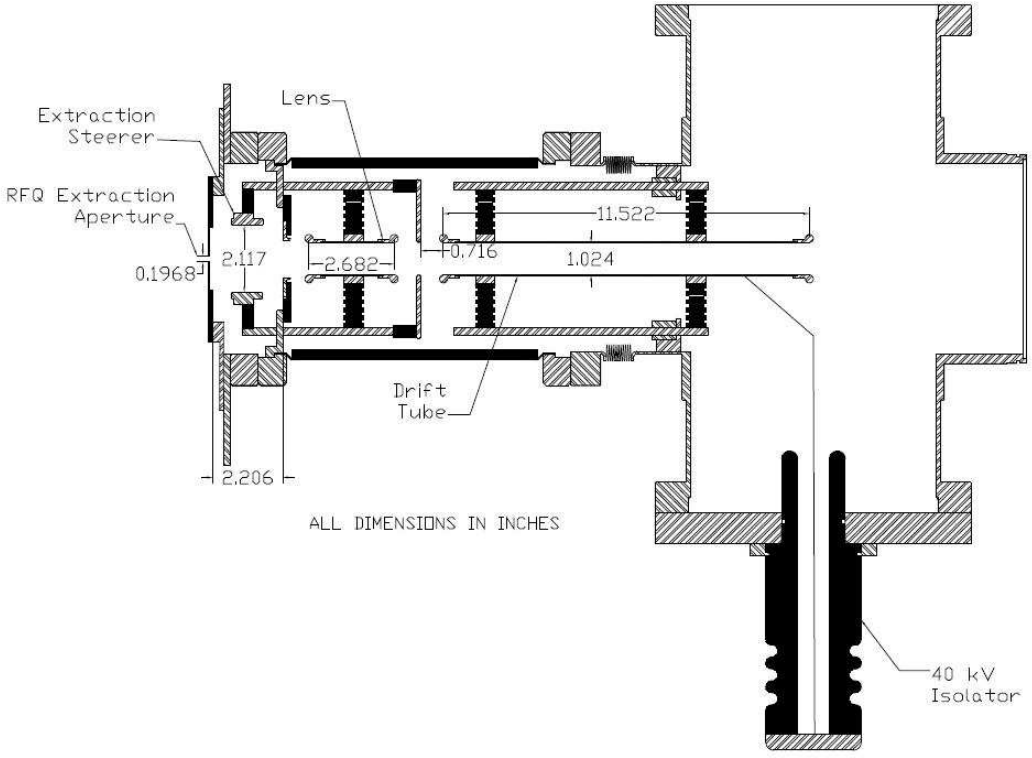

Figure 3–17: Schematic of the installed extraction optics.

The energy selecting drift tube is attached to a 60 keV voltage supply via a fast solid state (Behlke) switcher. This allows for the exit energy of the

ions to be carefully controlled. The ions enter the drift tube which is set at a potential, U_{cavity}. The tube is then pulsed down quickly (fall time $\approx 0.2\ \mu$s) to 0 V with the ion bunch inside. The ions inside the tube will not feel any effect of the switching and will exit the system with an energy given by q(U_{HV} - U_{cavity}) where U_{HV} is the bias voltage of the RFQ above ground, shown in figure 3-17 [35].

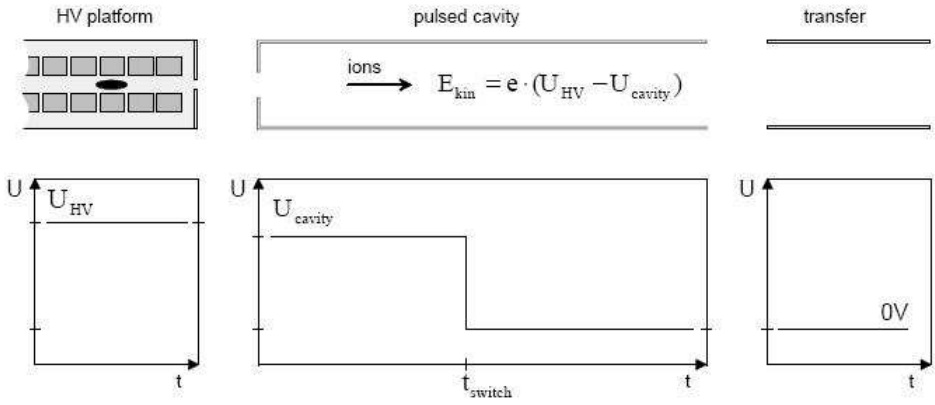

Figure 3–18: The voltage scheme of the energy selection tube giving a final energy to the ions of q(U_{HV} - U_{cavity}).

The tube is 30 cm in length, required to ensure that the entire ion pulse can be inside the tube before it is switched and does not exit during the switch down.

3.4.2 Ion Detection

Ions are detected at two different points in the test stand beam line. Above the 90 degree bender, there is a standard design Faraday cup for measuring the DC beam delivered from the ion source. This is used to measure how much beam current is being directed to the injection optics of the RFQ and is the basis of all efficiency measurements. After the RFQ extraction optics, a Faraday cup was used for tests of the device in DC transmission mode and a

microchannel plate (MCP) was used in its place for bunched mode operation. An MCP is a plate of lead glass with over 100 channels for electron multiplication, depending on the size of the plate. A thin metallic layer is applied to both sides of the plate so that a potential difference can be applied. An ion striking the channel will liberate an electron which will then be accelerated and multiplied through collisions with the channel walls [36]. The MCP assembly consists of two MCP plates (Delmar Ventures) in a chevron configuration and a phosphorus screen. This configuration maximises the signal gained from a single ion as it matches the channel locations on both plates. A commercially available assembly is shown in figure 3-19 [36]. The screen is not being used as an imaging device for these tests, so the voltage was applied as would be used for a metal anode configuration.

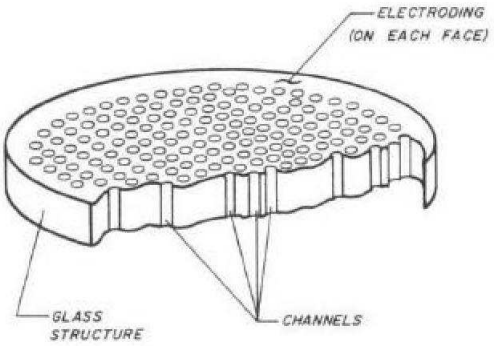

Figure 3–19: A microchannel plate.

3.5 Emittance Measurement

The emittance of the beam is measured using a deflection scanner of the Allison type [37]. The momentum is approximated by the velocity distribution of the ions, as they are non relativistic.

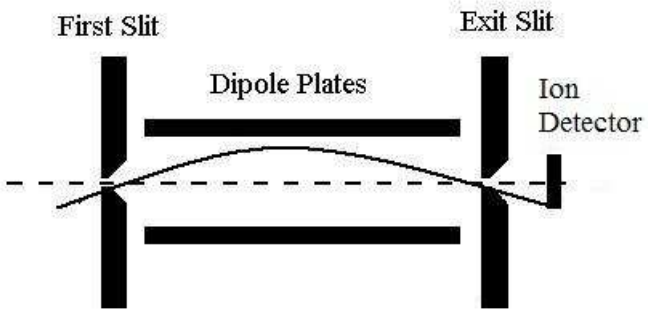

Figure 3–20: Schematic of the deflection emittance scanner showing a central line (dashed) and a typical ion trajectory (solid)

The deflection scanner consists of two narrow slits separated by two flat plates used to deflect the beam in between the two slits as pictured in figure 3-20. At a given spatial location within the beam envelope, the first slit will allow only a few ions of the beam along the x-axis to enter the scanner. A voltage is then applied to the plates in the range ±50 V in steps. Each time an ion pulse is ejected from the RFQ, a different voltage is applied. The amount of voltage applied to steer an ion through the second slit is related to the angle it is traversing by

$$x' = \frac{V}{\phi}\frac{L}{4d}, \tag{3.1}$$

where eϕ is the energy of the beam and L and d are the length and separation of the plates respectively and V is the voltage difference applied to the plates [37]. In our case, the length of the deflection plates is 69.85 mm and the separation between the plates is 4.0 mm. In a small angle approximation, this is equivalent to the transverse velocity of the ion. This is repeated for a series of position steps of the linear motion feed through. The emittance along that axis is then given by a rms analysis of the phase space plot. A mechanical

drawing of the scanner built for TITAN is shown in figure 3-21 along with a photograph of the device partially assembled showing the lower half of the slit assembly and the deflection plates.

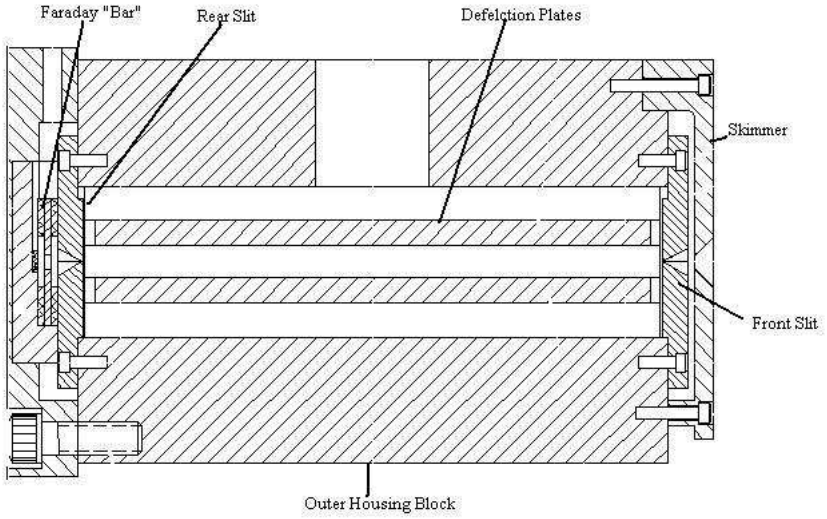

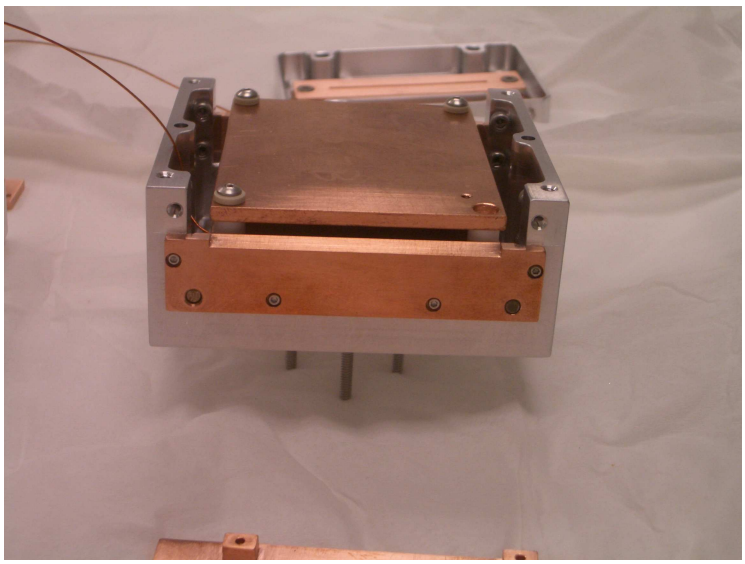

Figure 3–21: Schematic of the deflection emittance scanner used in the test stand (top). The deflection plates are 69.85 mm long. The Faraday detection electrode and rear casing were removed and a MCP detector placed at the exit of the device. A photograph of the scanner with the top half of the slit assembly and casing removed (bottom)

The maximum angular resolution of the device is dependent on the slit size by

$$\Delta\theta = \pm\frac{s}{L} \tag{3.2}$$

where s is the size of the slit that the ions pass through on entrance and exit.

The scanner is mounted inside an additional 8" (20.32 cm) cross attached to the exit side of the test stand. It hangs vertically from a motorised linear feedthrough and is adjusted to be perpendicular to the incoming beam. The bottom plate of the device is held at ground while a voltage is applied to the top plate. Both the motion of the feedthrough and the voltage applied are controlled by power supplies interfaced with the RFQ control system.

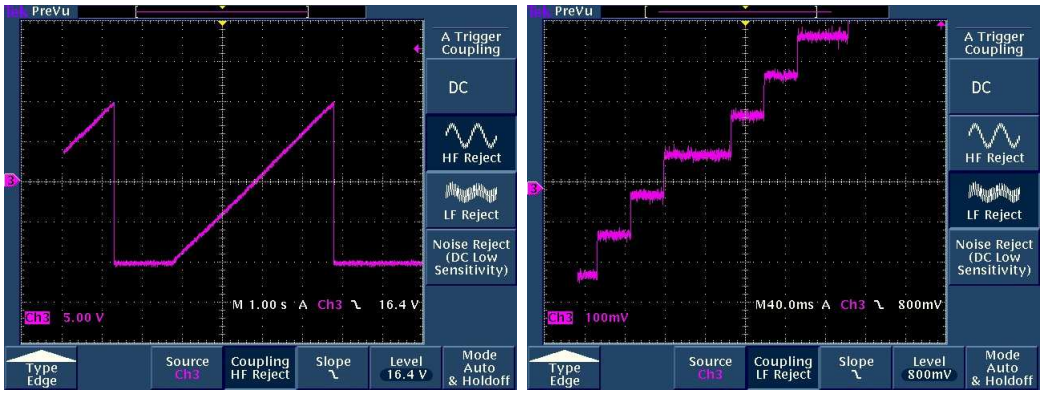

Figure 3–22: Voltage scan of the emittance scanner with a full voltage sweep (left) and an enlarged view of the voltage stepping (right)

Figure 3-22 shows an example of the voltage scan on the plates. The emittance rig moves to a new position for each sweep. In the shown close-up, one can see that some of the voltage steps were longer than others. This was used to diagnose a trigger delay that had been set incorrectly and was corrected for later scans. The scan was synchronised with the ejected ion pulse from the RFQ so that each pulse coincided with a new voltage setting. The transmitted ions strike an MCP mounted behind the scanner and the

relative signal strength is measured via a charge integrator with an allowed window of about 30 μs to make sure all the ions in a pulse were detected. The integrated signal was then saved in a data file for each scan.

In some cases, the scans were repeated several times and the results averaged to increase the signal-to-noise ratio. The main source of noise was line pickup on the integrator, the effects of which varied with the ejection pulse frequency of the RFQ (ie. the data taking rate compared with the noise frequency) and the RC circuit of the MCP detector set-up. A larger capacitance value reduced some of the integrated noise effects by increasing the rise time of the detected signal. This meant that once an ion pulse was detected, the variations of the noise were not detected until the longer rise time has passed. This increased capacitor value decreased the timing information that can be extracted due to a longer rise time for the signal. The start time of the signal and the strength of the initial pulse are determined by the ions, but the overall area is dominated by this long rise time. For the case of the emittance scans, this was allowable since the relevant information is the relative strengths of the ion generated signals and not the absolute number of ions and the total time extent of the signal is on the order of several microseconds, still less than the 30 μs data collection window.

The emittance scans were performed under a variety of conditions. By varying the input ion current as well as gas and voltage parameters of the RFQ, the scans characterise the effect of these changes on the emittance of the beam.

CHAPTER 4
Experimental Results

To test the operation of the RFQ and find its optimal parameters, two main aspects are considered. The first is the overall efficiency. As has been stated previously, one of the primary concerns is how many ions are lost in the system since experimental operation will include cooling of ions produced at low yields. Secondly, the transverse emittance of the beam as it exits the device was examined. A smaller emittance will lead to easier manipulation and transport of the beam through subsequent elements.

The main factors that will affect both the transmission efficiency and the emittance are the buffer gas pressure, the q value of the RFQ, and the amount of time the ions spend in the device. The ejection pulse strength out of the trap and the exact DC slope of the RFQ electrodes were observed to be secondary effects on the emittance and were not examined in detail. Data were taken at the RFQ test stand with a ^{133}Cs stable ion source.

4.1 Simulations

Simulations of the test stand optics and the RFQ [24] were performed with the SIMION software [38] using a Monte Carlo code to approximate the motion of ions in the gas during their time in the RFQ device.

Three simulation regimes were implemented – one with only the injection optics up to the entrance of the RFQ, one with the ions started from a point just outside the RFQ and followed through to the end of the extraction optics section and one with the whole system in place to ensure consistency.

The two main considerations were the acceptance of the device and the emittances both before and after the RFQ. The acceptance was found for the RFQ/deceleration optics (after the 90 degree bend) as these elements will be the ones implemented in the final TITAN setup. The results of the acceptance SIMION simulations are shown in figure 4.1 which shows a useful acceptance of 77 π-mm-mrad at 40 keV [24].

The simulations for the emittance were carried out assuming that the ions originated from the surface of the source with a thermal distribution of energies centered at 2400 Kelvin. The ion trajectories were then found for a distribution of 1000 ions. The matching of the emittance of the beam to the acceptance of the injection optics is shown below in figure 4-1 [24]. The overlap indicates that in the simulation, very little ($\approx 9\%$) of the beam was lost in transport to the deceleration optics.

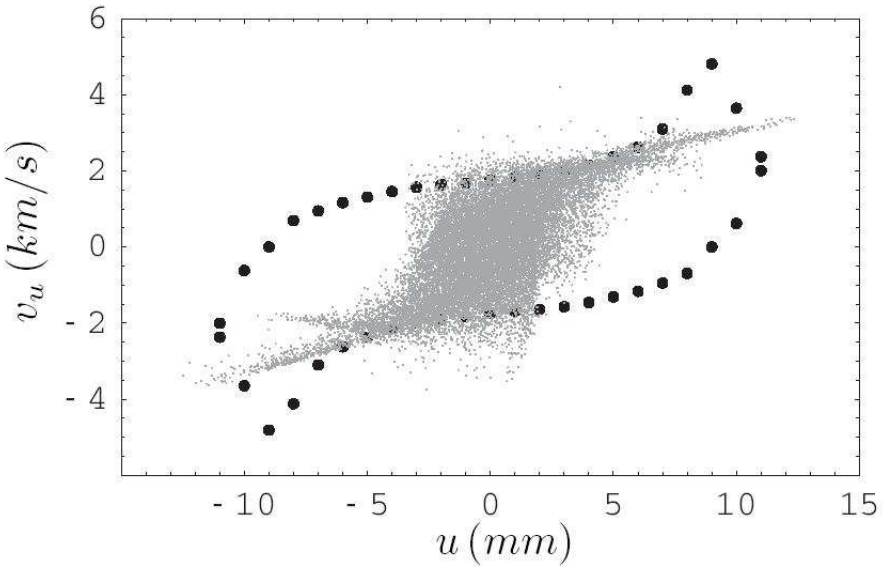

Figure 4–1: Comparison of the calculated acceptance of the injection optics (shown by black dots) and the simulated incoming emittance (grey).

The transverse emittance of the beam exiting the 90 degree bender were 45.9± 0.4 on the x axis and 7.16±0.2 π-mm-mrad on the y axis with respect to the beam direction z.. The difference in the two directions comes about due to the inherently non-symmetric field of the 90 degree bend. This matches up very well with the acceptance of the injection optics and deceleration region shown in Figure 4-1. The deceleration process is non-conservative and can therefore increase the emittance of the beam. It was calculated that upon entering the RFQ, the emittances would be 1085.0±0.2 π-mm-mrad and 495.0±0.2 π-mm-mrad with an overall efficiency of 64% [24].

The simulations of the full system were carried out using a viscous drag model for the movement of the ions through the buffer gas that compared well with experimental data of the mobility of cesium ions in helium. Various parameters were optimised, yielding values of q=0.4 at an RF of 400 volts and an electric field gradient of 0.1 V/cm applied through the non trapping region of the RFQ. As well, the helium gas pressure was set at 2.5 Pa as this is in the range with maximum cooling and minimum losses.

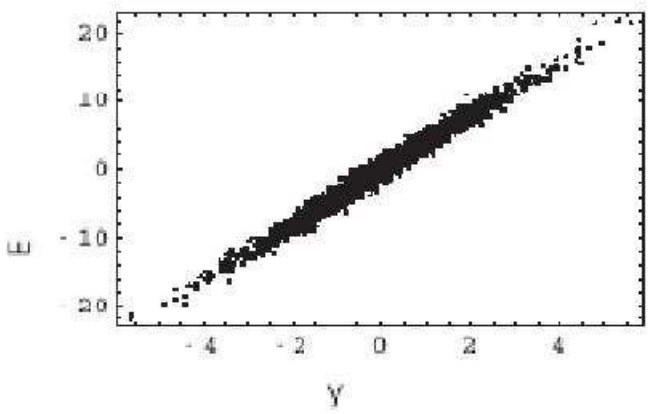

Figure 4–2: Simulated emittance ellipse extracted at 2.5 keV.

A typical result for the simulated emittance after the beam leaves the extraction optics is shown in Figure 4.2. In this case the pulsed drift tube was set to give a final beam energy of 2.5 keV. The simulated emittance here after cooling is 4.8±0.2 π-mm-mrad [24].

One of the studies performed was to determine the effect of the ejection strength on the emittance of the extracted beam. The ejection from the trap is determined by switching the voltage on two segments of the RFQ to create a potential leading out of the trapping area. The three end trapping electrodes and the corresponding potential well is shown in Figure 4-3. The amount by which these two segments were changed was investigated and the results shown in table 4.1.

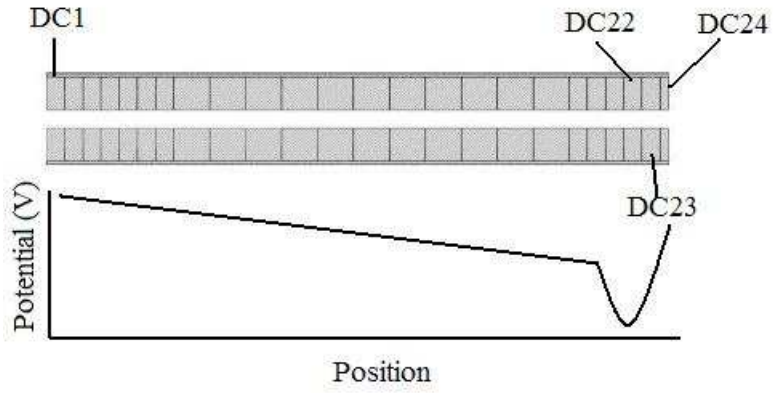

Figure 4–3: The DC potential applied to the electrodes and the trapping region generated by the last three electrodes (DCs 22, 23 and 24).

ΔV DC22 (V)	ΔV DC 24 (V)	ϵ (π-mm-mrad)
0	-30	3.3±0.3
0	-60	4.2±0.1
30	-30	3.8±0.2
60	-60	3.6±0.1
500	-500	4.8±0.2

Table 4–1: Ejection parameters and simulated emittances

The simulations showed that the beam could be transferred to the RFQ efficiently and that the expected emittances upon exiting the extraction optics and drift tube are between 3 to 5 π-mm-mrad at 2.5 keV. The experimental results will compare the predicted and observed efficiencies and emittances.

4.2 Transport Efficiency

To determine the efficiency of the device, we had to compare the pulse output seen on an MCP (microchannel plate) detector to the current measured at the Faraday cup just above the 90 degree bender. This meant that we needed to find a correlation between the MCP signal and the number of ions that had hit the detector. We also needed to determine if any beam was lost on the second leg of transport before the RFQ. The latter would let us find an efficiency result independent of whether the transport was affected by the direction of the beam exiting the bender.

The efficiency of the ions through the RFQ can be broken up into two parts. The first is the efficiency of injection into the RFQ and the second is the transfer through the RFQ in both DC and pulsed modes.

4.2.1 Injection efficiency

To measure the injection efficiency, we removed the RFQ structure from the system and placed a Faraday cup inside the vacuum chamber just after the entrance aperture of the RFQ portion of the setup. By measuring the current on the cup inside the box relative to the cup above the 90-degree bend, we determined how much of the beam was entering the RFQ aperture (see Figure 3-7). The aperture is only 4mm in diameter, so finding the best settings to allow for maximum acceptance is crucial.

Because of the possible fringe fields present from the high voltage plane of the entrance, a study of the effect of the boosted injection energy was done.

The data show that as long as the injection energy is 20 eV or higher, an injection efficiency of at least 90% is achieved as seen in Table 4-2. However, these data were taken without any buffer gas present in the system. With the gas present, a higher injection energy would be required to offset any scattering. In the performed SIMION simulations, the added buffer gas caused losses of only a fraction of a percent as long as the injection energy was high enough to allow admittance. A higher injection energy reduces the interaction cross section with the gas atoms and makes it less likely that the ions will scatter before entering the RFQ.

Injection Energy (eV)	Total current (nA)	Percentage Entering RFQ Housing
10	2.59	76
20	3.15	91
30	3.46	95
40	3.98	96

Table 4–2: Injection efficiency into the RFQ at 30 kV

The optimal injection efficiency was achieved with the following parameters for a bias potential of 30 kV. It was found that the injection optics underwent sparking too frequently when gas was added to the system so the energy of the ions was lowered to 5-15 kV and the electrode voltages scaled accordingly for subsequent tests. The injection optics have been redesigned for installation in the ISAC experimental hall with a cone-shaped electrode replacing the deceleration plates. This new design will not require high voltage wires to be so close to the RFQ, so it is expected that ion beams up to 60 keV can be injected from the ISAC beam line with little sparking.

The parameters for the most efficient injection into the RFQ are shown in Table 4-3. It shows the settings of the first quadrupole triplet (Q1, Q2), the 90 degree bender (QB3±), the quadrupole triplet after the bend (Q4, Q5) and the two deceleration electrode plates before the injection plane (Decel1,

Decel2) shown in Figure 3-4. It was found that no steering correction was required for the results shown in Table 4.2.

Optical Element	Voltage(V)
Q1	2620
Q2	3870
QB3+	26050
QB3-	26100
Q4	2410
Q5	4860
Decl1	12010
Decl2	3400

Table 4–3: Injection efficiency ion optics settings at 30kV

These results were relatively stable to small changes in beam optics. For example, 85% of the beam entered the RFQ cavity if the deceleration plates were adjusted to voltages of 9800 and 12000 with 30 eV injected energy.

4.2.2 DC transport

To determine the efficiency of the RFQ in DC mode, a Faraday cup was placed after the exit of the RFQ to measure the DC current of ions that passed through the RFQ. In this case, the DC potentials on the RFQ electrodes were set to provide a small gradient toward the exit and no longitudinal trapping potential was applied. The applied RF was set at 420 V and 690 kHz giving a q value of 0.32. The current exiting the RFQ was then compared to the total current measured if the beam was directed to the Faraday cup above the 90 degree bender. We were also able to measure the beam current striking the entrance plate of the RFQ box to determine if the settings for maximum transmission through the RFQ had the same efficiency as the settings for maximum entrance into the RFQ area.

Gas Pressure (Pa)	Injection Energy (eV)	Total current (nA)	Percentage at Exit
5.3 x 10^{-5} (He off)	100	10	65%
0.23	100	10	60%
0.23	40	10	64%
5.3 x 10^{-5} (He off)	26	12.7	60%
0.48	26	12.7	50%

Table 4–4: DC mode efficiency

Table 4-4 lists the percentage of the measured beam above the 90 degree bend as the gas pressure and the boosted injection energy are varied. The data were taken with an incoming ion current of close to 10 nA which should not saturate the RFQ in continuous mode. The data show that the measured DC mode efficiency is close to 60%. This is provided that the injection energy is high enough to overcome the buffer gas scattering on entry as previously discussed. It is obvious here that at an energy of 26 eV scattering reduces the overall efficiency. Not much effect was seen from the different gas pressures, indicating that not much scattering is taking place in the transfer of the ions through the RFQ at these pressures.

4.2.3 Bunched mode transport

The efficiency of the RFQ in bunched mode cannot be determined using a Faraday cup as it is a relatively slow measure of the average beam and cannot handle short pulses. We therefore used an MCP detector placed after the energy selection drift tube. To use this method, we first had to calibrate the MCP to be able to determine an approximate number of ions from the signal we observed. This test was performed by placing the MCP after the second set of quadrupoles that sit just after the 90 degree bend. One of the the inputs for the bender was then connected to a power supply via a simple gate circuit set with a window of 100 μs. Thus two of the four electrodes in the bender were permanently set to the correct settings to bend the beam and

the other two only had the correct voltage during the 100 μs window. Making the assumption of minimal losses during bending, this gave a pulse of beam that could easily be compared to the beam current striking the Faraday cup above the bender by setting all the bender voltages to zero. The area of the oscilloscope trace was then compared to the current measured from the source.

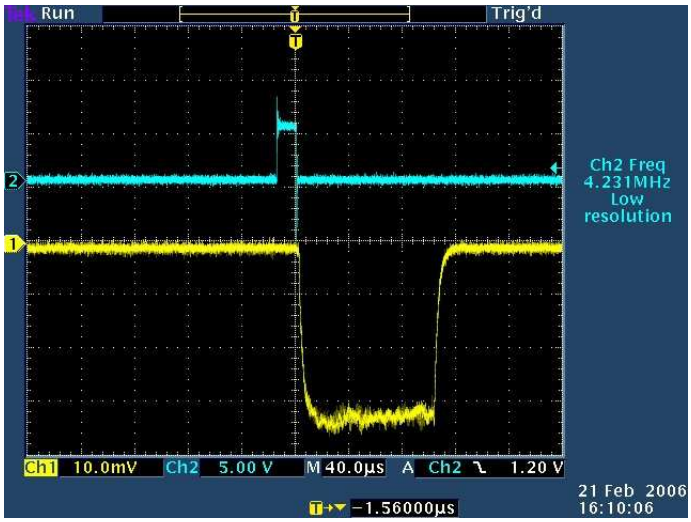

Figure 4–4: Example of MCP calibration data

Figure 4-4 shows a sample oscilloscope trace for MCP calibration. The top trace is the trigger to the switched bending electrode. The beam was allowed to progress for 100 μs after this trigger. The bottom trace shows the response of the MCP filtered through an RC circuit. The area of the MCP trace on the scope was compared with a calculation of the number of ions that would be incident during the pulse at the measured ion current.

Current (nA)	Time (μs)	Area of MCP trace (mVμs)	Number of Ions/Unit Area
0.12 $\pm$0.01	100	3200	23.5 $\pm$ 2
0.30 $\pm$0.01	100	6222	30.2 $\pm$1
0.72 $\pm$0.01	100	14857	30.3$\pm$0.5
0.05 $\pm$0.01	100	1503	20.8$\pm$4

Table 4–5: MCP efficiency

Table 4-5 gives the average number of ions per unit area (mVμs) as 26$\pm$2. Using this value, we can look at the effect of varying the buffer gas pressure, cooling time and RF parameters. With this information, tests of the properties of the RFQ in bunched mode were performed with a continuous input beam.

Buffer Gas Pressure

The buffer gas pressure determines (along with the DC field gradient applied) the time it will take for the ions to cool. A higher pressure will result in more ion-gas collisions in a given time and therefore reduce the time required to achieve a cooled state. But an increased gas pressure also increases the probability of scattering out of a stable trajectory. During testing of the RFQ, we first used neon as a buffer gas to ensure that we would be able to stop the ions properly. Although helium was used for all subsequent data, the effect of the gas pressure on transfer efficiency was determined for both helium and neon gas.

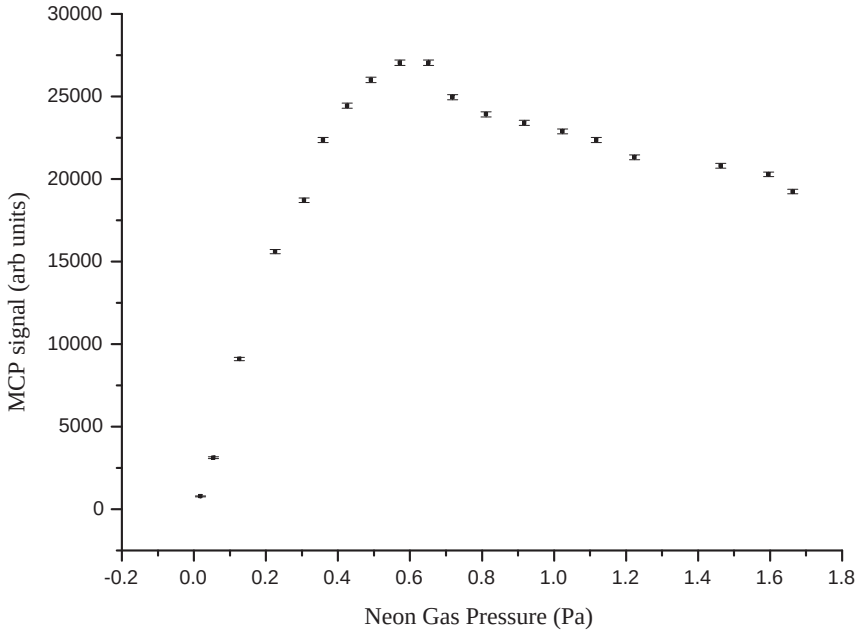

Figure 4–5: Effect of neon gas pressure on transmission

Figures 4-5 and 4-6 show the number of transmitted ions calculated from the generated MCP signal and the calibration data as a function of increasing gas pressure inside the RFQ. The pressure is measured using a cold cathode gauge mounted on the lid of the RFQ structure approximately 20 cm from the exit aperture. The ions are ejected from the RFQ at 30 Hz in both cases. The incoming ion current was 70 pA for the neon gas and 0.35 nA for the Helium gas. The electronics of the detection circuit for the mcp were changed slightly after the tests with the neon buffer gas were complete. Therefore the calibration that was performed is not valid for the neon gas data and relative signal strength must be used in that case.

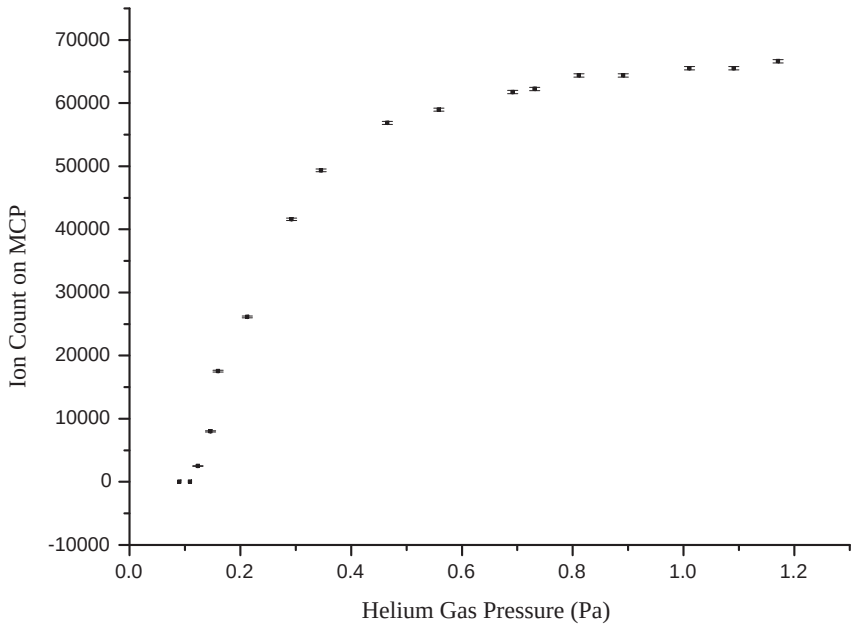

Figure 4–6: Effect of helium gas pressure on transmission

The beam energy for these tests was 5 keV and the injection optics were scaled accordingly. Specifically the deceleration plates were set at 1950 V and 500 V respectively which should give an injection efficiency of at least 80%

Since this was the first use of the RFQ in bunched mode, many adjustments were necessary before an optimal signal was achieved. The RF voltage on the RFQ was set to 396 V at 654 kHz giving a q value of 0.34. The DC potential inside the RFQ was set to a slope of 12 V across the first 23 electrodes (DC1 = +12 V with respect to the RFQ bias) and the last electrode was switched from +230 V to -100 V for the trapping and release of the ions. This generated a shallow well potential for the first tests that was relatively insensitive to the issue of how quickly the pulse is ejected.

The ejection optics were also adjusted to give maximum signal. The optical elements in the ejection section are sequentially the segmented steering

tube, two acceleration plates separated by a short drift tube and the long drift tube (see Figure 3-17). The long drift tube held a static voltage giving different optimal results than the simulation showed. The optimal settings for this set-up had all four parts of the steering tube set at -1000 V with respect to the HV Bias, the acceleration plates at -1000 V and -975 V respectively and the short drift tube at - 380 V. The long drift tube is set referenced to ground and is at 4850 V (-150 V with respect to the HV).

For the helium gas pressure data, the DC slope of the RFQ was adjusted to give a slope of 4 V over the first 21 electrodes and the remaining 3 were used to create the potential well with voltages of -17 V, -10 V and +90 V during trapping and +110 V, -10 V and -26 V to eject the ions. All other parameters remained the same.

Figures 4-5 and 4-6 show that in both cases, the efficiency increases with pressure until a plateau is reached. This plateau occurs when the cooling effects of increased pressure start to be balanced by the increased probability of scattering too far off axis. When the pressure is increased further, the scattering effects begin to dominate and more ions are lost within the RFQ. This current decrease can be seen in the data for the neon buffer gas which is heavier, but a high enough pressure to see this effect was not achieved with the helium.

In the case of the neon buffer gas, the best operating pressure for transmission of the cesium ions was in the range 0.5-0.7 Pa, while for the helium gas a pressure of at least 0.6 Pa was needed and very few losses were observed up to a pressure of 1.2 Pa. Pressures higher than this were not achievable with this setup due to insufficient differential pumping in vacuum sections outside the RFQ tank.

DC Potential and Trap

The electric field will affect the speed at which the ions move through the structure. The ions must be pulled through the gas such that ions that are cooled either in the first or subsequent passes are still funneled to the trapping region. Those that are not will be ejected and this will decrease the efficiency. We found that a gradient of about 4 V across the 21 non trapping electrodes was sufficient giving a gradient of 6 V/m at an injection energy of 30 eV.

The other aspect of the DC that will have an effect is the potentials applied to the last three electrodes. During accumulation these will control the depth of the potential well for the ions which will determine the temperature that can be reached and the types of losses that will occur. If the well is too shallow, ions may not be trapped and will be lost and if the well is too deep the space charge induced losses will be greater

The effect on the number of output ions can be seen in Figure 4-7. The data were taken with an input current of 50 pA and a buffer gas pressure of 0.4 Pa. The ions were ejected from the trap at a 15 Hz rate. The depth of the well is determined by the negative voltage applied to segment 22 during collection measured with respect to the voltage applied to segment 21. A higher voltage gives a deeper trap. The data show that at low voltages, below 12 V, the ions are not transmitted very well and there are many losses. At voltages larger than 17 V depth, the transmission starts to drop off again. The effect of the potential applied to the other well electrode (segment 23) was also investigated, but it was found to be less important as the total potential at that position is dominated by the "barrier" potential applied to the last electrode (segment 24) which we found needed to be about 90 V above the segment 21 baseline to ensure minimal losses.

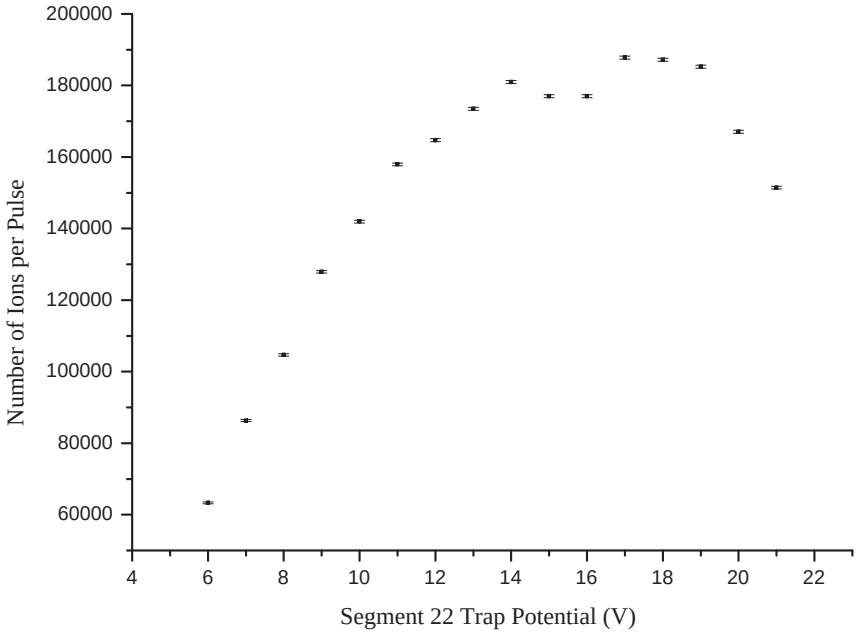

Figure 4–7: The number of ions exiting the RFQ as a function of trap depth determined by RFQ segment 22

The effect of the potentials applied to these electrodes during ion ejection was also examined but little effect was seen. It is thought that the ejection will have an effect on the emittance of the ejected ions but will not greatly affect their ability to leave the device.

Time in Trap and Ion Trap Density

The length of time the ions spend in the trap is an important parameter to consider as we are intending to work with short-lived isotopes. The minimum time to achieve the necessary cooling will depend on the buffer gas and the species of ions, but the trend of the efficiency with increasing cooling times is expected to be very similar for all ions. The ions must be in the trap long enough for effective cooling, but a long trap time will increase losses due

to collisions and space charge effects. Also, the continuous loading of the RFQ means that more ions will be in the trapping region for lower ejection frequencies for a given input current.

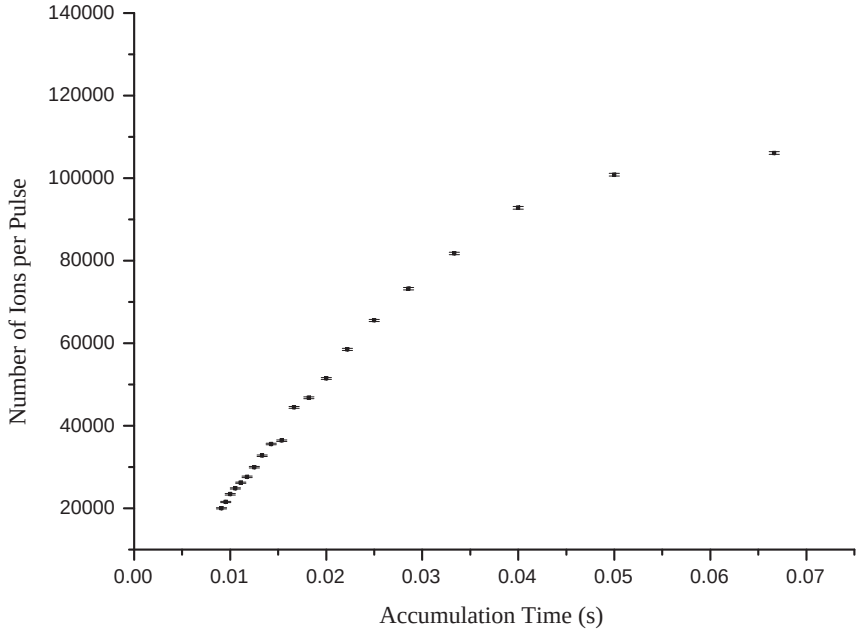

Figure 4–8: The effect of accumulation time on the efficiency of the RFQ

Figure 4-8 shows the effect of the length of time the ions are stored in the RFQ has on the output number of ions. To characterise the behavior of the ions the frequency of ejection from the trap was varied to determine its effects. Making the assumption that the ejection of the ions is fast the time the ions spend cooling in the trap is then the reciprocal of the ejection frequency. This is valid as the minimum time spend in the trap is 10 ms and the ejection takes place in less than 2 μs. The data were taken with an incoming ion current of 330 pA or 2.6x10^9 ions per second with a helium gas pressure of 0.48 Pa. All other parameters remain unchanged from the helium pressure measurements. The plot shows the number of ions detected at the MCP as a function of the

time that the ions are allowed to accumulate in the RFQ with continuous filling.

The data trend to a straight line for times less than 33 ms (f>30 Hz), indicating that the efficiency of these shorter times is the same. The data tend to show fewer output ions for the same input current for times longer than 33 ms (f<30 Hz). While it is impossible from data on the number of ions to determine if the ions have become cooled, this indicates that the range of 30 - 110 Hz presents no difficulty for the efficient ejection of the ions.

The space charge limit of the RFQ in bunched mode was calculated to be on the order of 10^7 ions [24], meaning that for times longer than 10 ms (f<100Hz) the number of ions entering the trap is higher than the maximum number that can be cooled and this will affect the number that are lost. However the slope of this linear section can give an indication of the experimental space charge limit. If the incoming current were lower, the slope of the line would reflect the number of ions exiting per second in comparison with the known input, yielding a value for the efficiency of the device. In this case, the efficiency is not known, so the slope can be used to find a lower limit for the space charge limit by assuming 100% transmission efficiency and using the slope to determine the number of useful (not lost) incoming ions. Fitting a line to the linear section yields a slope of 2.9×10^6 ions per second. A lower limit for the maximum number of ions held in the trap is determined by the slope and the longest cooling time in the linear portion, giving a value of 9.6×10^4 ions if 100% efficiency is assumed.

q-Value and RF parameters

To test the effect of the RF parameters on the efficiency of the RFQ, the signal of the ejected ions on the MCP detector was measured using an

incoming ion current of 75 pA and a gas pressure of 0.48 Pa. The injection and extraction optics as well as the DC potential of the RFQ were set as before. Since the q value of the RFQ depends on both voltage and frequency, varying both yields a more complete picture of the overall effects.

Keeping the frequency of the applied voltage fixed at 659 kHz, the voltage was varied from 200 to 320 V in steps of 10 V shown in Figure 4-9. The data show a peak at a q value of 0.21 corresponding to a voltage of 250 V. This was much lower than the simulated optimal q value for the RFQ, which was close to 0.39 [24]. The apparent discrepancy is due to the calculated optimum giving a low emittance of the transmitted beam, whereas the data in this section of these results are related to the transmission efficiency only. The motion of the ions in the RFQ should be stable above a q value of 0.1 but may not be cooled efficiently. The transmission is seen to be better at lower q values but the emittance of the extracted beam will be worse. At q values lower than 0.1, the ion amplitudes of the ion trajectories are too large and trapping does not occur.

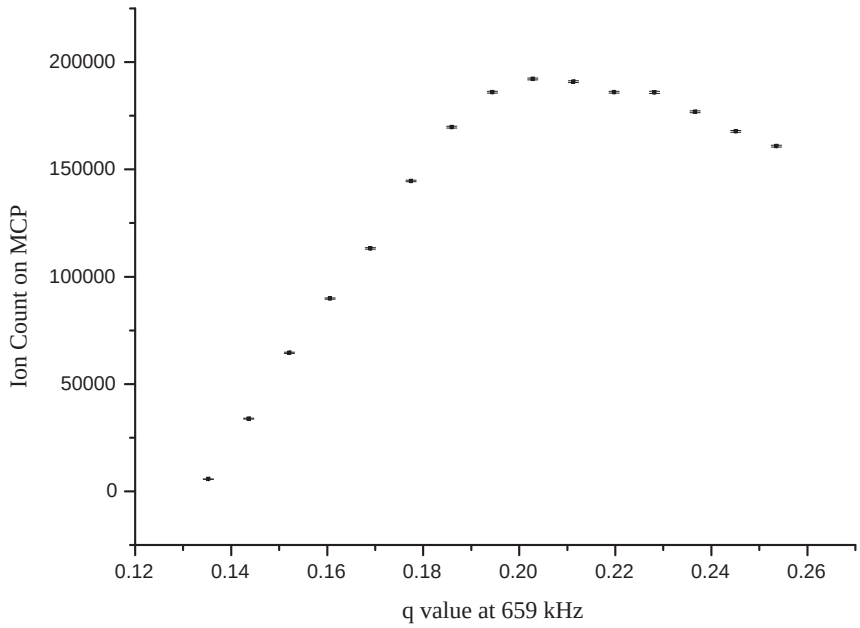

Figure 4–9: The transmission of ions through the RFQ as affected by the Q value at fixed frequency (659 kHz)

Figure 4-10 shows data taken at a constant voltage of 300 V varying the frequency from 600-750 kHz. It shows that the transmission of the ions increases as the q value is increased up to at least q =0.31. Data were not obtained for higher q values at this voltage. Though the maximum transmission at fixed voltage was not determined, it is clearly at a higher q value than the fixed frequency data. This gives an indication that the slightly higher voltage used in the second case will be more advantageous for operation as the maximum transmission optimum is closer to the expected emittance optimum. As the goal is to maximise the efficiency and minimise the emittance, settings that give optimums in both these areas are desired.

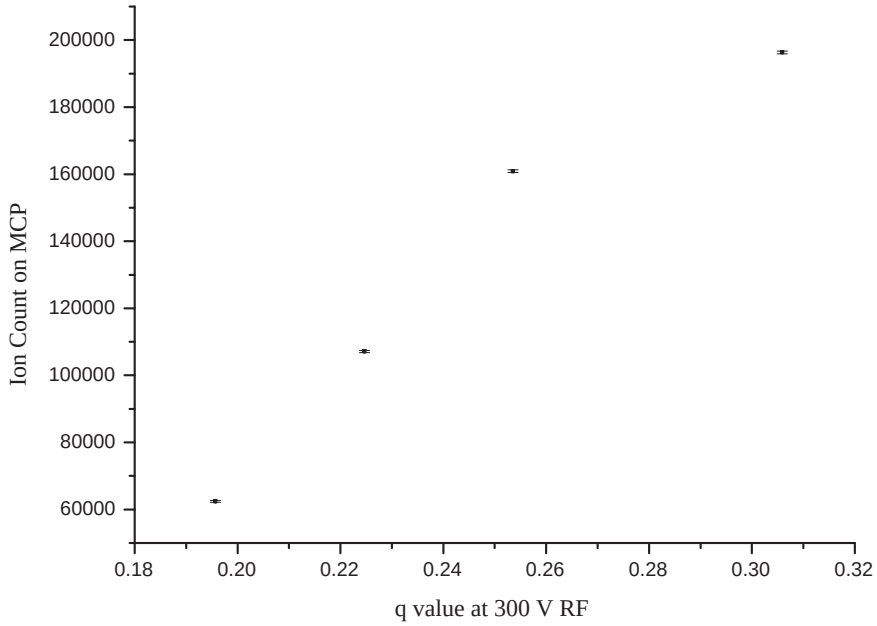

Figure 4–10: The transmission of ions through the RFQ as affected by the Q value at fixed voltage (300V)

4.3 Transverse Emittance

The transverse emittance of an atom or ion beam is a measure of the divergence of the beam envelope in the directions perpendicular to the beam. This is usually dealt with in cartesian coordinates. We expect the beam to be circularly symmetric in size and emittance as all the beam elements after the RFQ are cylindrically symmetric. To this end we measure the transverse emittance on one axis and use this as a reasonable approximation to the 'true' emittance in both planes.

4.3.1 Emittance Determination

To determine the emittance, the emittance meter (see section 3.5) was coupled with an MCP and a charge integrator placed after the long drift tube

at the end of the extraction optics that measured the relative intensity at each position and voltage step. These relative intensities were then fed into a program in MATLAB written by R. Baartman (see Appendix A). This program plots the intensities and then takes user inputs to define a rectangular area where the beam is present. Once this is defined, the program finds an average of the points outside the designated beam area and uses this as a background. The background is then subtracted from all points and the variation of the points outside the defined beam area is used to define the standard deviation of the noise, which is used as a cut value. Anything less than this cut value is discarded and the points set to zero throughout the whole plot. This method introduces a bias so that the reported emittance is always lower than the true emittance. The standard deviation of the noise is used to estimate this effect using the inflation factor. An emittance ellipse is then calculated using just the remaining points. This can be fine tuned by using an additional interactive cut tool to eliminate islands in the background.

The three steps are shown below with the raw data pictured as a contour plot and the initial cut and subsequent final result show in the latter two frames. In Figure 4-11, the first picture shows a contour plot of the signal height plotted with the position on the horizontal axis and the angular displacement on the vertical axis. The second picture shows the data after both the cut and manual removal of spurious non-beam islands. The white line indicates the fit of the emittance ellipse.

The output of the program gives the parameters of the calculated emittance ellipse. It shows the position extent (x), the angular extent (θ), and a parameter r_{12} which determines the rotation of the ellipse from the horizontal. These three numbers completely define the ellipse and the emittance is then

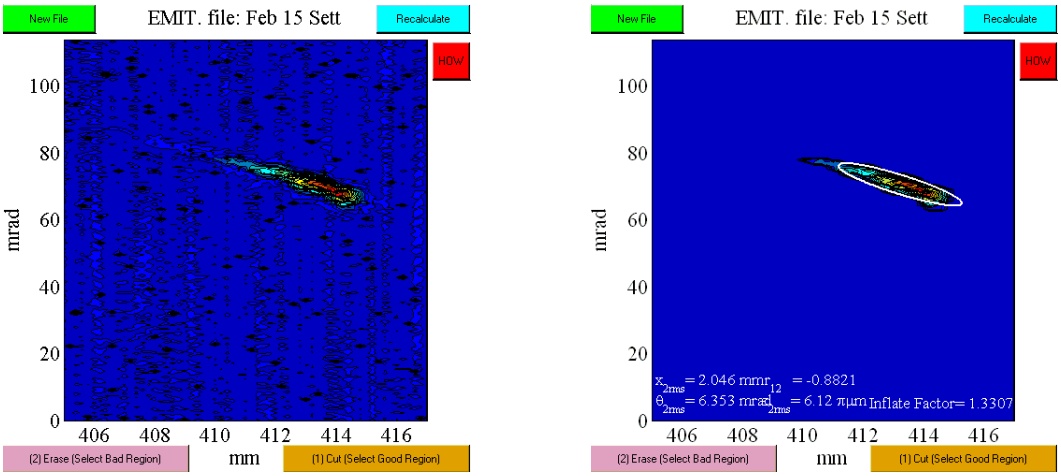

Figure 4–11: Example of emittance determination routine with the angular extent on the vertical axis and the position extent on the horizontal.

calculated from these parameters using

$$Area \approx \pi \cdot x \cdot \theta \cdot tan(r_{12}) \tag{4.1}$$

for small values of r_{12} and equation 2.35. An example of typical emittance parameters is shown in Table 4-6.

Frequency(Hz)	Emittance (π-mm-mrad)	Inflation Factor	x(mm)	θ(mrad)	r12 (mrad)
30	19.6	1.2071	3.838	11.73	-0.9008
40	16.1	1.1494	3.481	10.60	-0.8996
50	15.6	1.1407	3.515	10.57	-0.9062
60	14.5	1.1611	3.394	10.22	-0.9087
70	13.9	1.1175	3.432	10.15	-0.9168
80	15.4	1.1273	3.523	10.16	-0.9025
90	14.1	1.1075	3.594	10.41	-0.9269

Table 4–6: An example of emittance parameters

The emittance is calculated for a 2σ confidence level assuming an ideal elliptical shape for the emittance. The 'inflation factor' given is an estimate of how much the emittance is underestimated due to the noise cut. While there are other factors involved in calculating the emittance, the possibility of excluding some points that are beam in the cutting process of the calculation dominates the potential error. The inflation factor is given by:

$$Inflation = \frac{pfac}{pfac - (1 + log(pfac))} \tag{4.2}$$

where pfac is the peak value of the beam data divided by the standard deviation of the noise.

The true emittance is between the calculated value and that value multiplied by the inflation factor. Data that had an inflation factor of more than 1.5 were discarded as they were judged to be too noisy to be trustworthy. This only became relevant in the examining the effect of the q value with a slow 30 Hz ejection where it was not possible to obtain clear results for half of the 400 V data. The inflation factor is represented in the subsequent measurement data by showing upper error bars of the maximum value of the emittance calculated by multiplying the measured emittance and the inflation factor. The statistical variations are due mainly to the mechanical resolution of the meter.

The angular resolution is given by

$$\Delta\theta = \pm\frac{s}{L} \tag{4.3}$$

where s is the slit width of the entrance and exit of the device and L is the total distance between the two slit planes. The spatial resolution is taken to be 0.1 mm which is half of the movement step size to account for mechanical resolution of the motor and the rotary motion feedthrough.

As in the case of the efficiency measurements, we looked at the effects of various parameters (buffer gas pressure, q value, cooling time) separately. The emittance data were taken with a bias potential of 5 kV and the energy selection drift tube set for the final ion energy of 4 keV. The DC potentials on the RFQ were not varied during the tests. The first 21 electrodes were not individually set in this case but were controlled via a resistor chain that had the first segment at +4 V with respect to the HV bias and the 21st segment at -1 V. The three remaining segments defined the trapping region such that segment 22-24 were -17 V, -10 V and +350 V respectively during trapping and +90 V, -10 V and -16 V during ejection. The emittance was determined as a function of the helium gas pressure, the stability parameter q, and the frequency of ion ejection or cooling time.

4.3.2 Effect of helium Gas Pressure on Emittance

Emittance measurements for the buffer gas pressure effects were only performed with helium gas and not with the neon buffer gas. The data were taken with an incoming ion current of 5 pA at an ejection rate of 30 Hz. The applied RF had an amplitude of 400 V_{pp} at 659 kHz corresponding to a q value of 0.34.

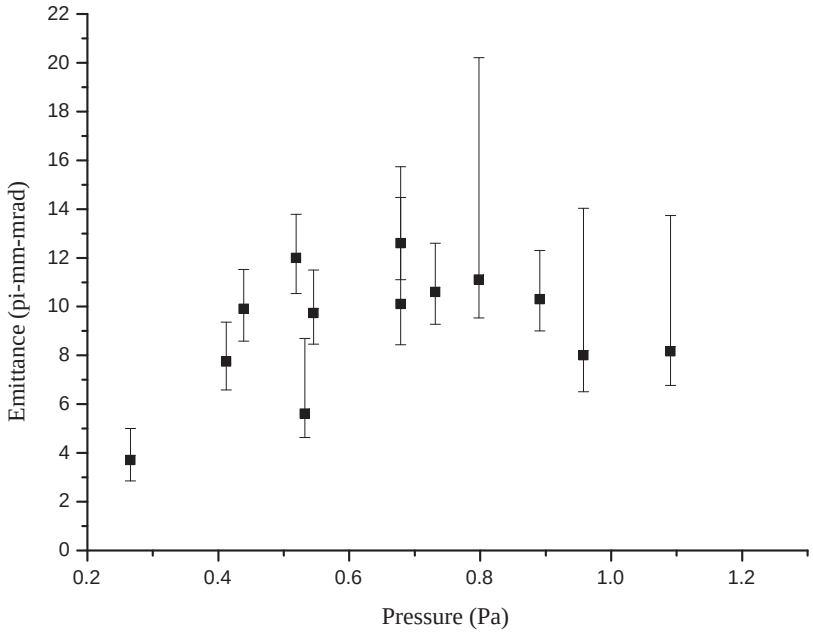

Figure 4–12: Emittance effects of increasing helium pressure at fixed RF parameters

The data in figure 4-12 show an increase in emittance with higher pressure up to 11 π-mm-mrad at 0.6 Pa before leveling off and perhaps dropping off again slightly. When this is combined with the efficiency data in section 4.2.3 which gives lower transmission for pressure less than 0.533 Pa, a pressure above 0.7 Pa would seem to be preferable. In taking this data, we could not go above 1.2 Pa due to sparking of the deceleration electrodes.

4.3.3 Q value

The effect of the stability parameter of the RFQ was studied by varying the frequency of the applied RF voltage within the range 600-750 kHz while keeping the voltage applied in the range 350-400 V. To vary the voltage too much would affect the acceptance of the RFQ as well as the behavior of the ions within the device and is not what we were interested in. One value was

taken at a voltage of 200 V with a frequency that gave a comparable q value in order to show that the higher RF voltage is more effective in confining the ions and achieving better cooling.

The data were taken at three different frequencies of trap ejection (30, 60 and 90 Hz) at incoming ion currents of 20-40 pA and a helium buffer gas pressure of 0.8 Pa to show how the axial confinement of the RF interacts with the time the ions are in the trap resulting in the final cooling state. The results of the tests for 60 Hz are shown in figure 4-13 below.

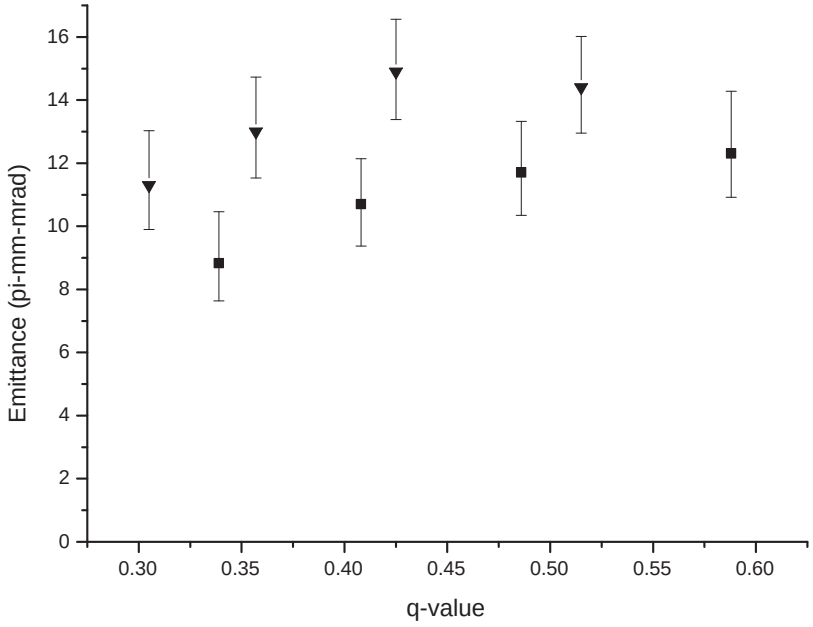

Figure 4–13: Effect of q value on emittance for 60 Hz pulse ejection at 350 V (triangles) and 400 V (squares)

To achieve the range of q values seen in the figure, the frequency of the applied RF voltage was varied under two different voltage values (350 and 400 Volts). This gave two curves on the plot with the 4 data points corresponding to the 400 V data (squares) consistently lower than the 350 V data points

(triangles). These data then indicate that a higher confining voltage reduces the overall emittance, which is consistent with calculations and simulations. In this case both data sets trend in the same direction giving lower emittances for lower q values. This is contrast to the calculated best q value of 0.39 discussed briefly in section 4.1 (see also [24]).

Figure 4-14 shows the emittances achieved for q values in the range 0.3-0.6 for ejection rates of 30 and 90 Hz. The same effect of dual curves was seen with these two data sets as was seen with the 60 Hz data. In the case of 30 Hz ejection from the trap, increased q value seems to give lower emittances. This indicates that the longer the ions are in the trap, the more the induced motions of the RF will affect the final cooled state. This will influence the low q (high frequency) data more than the high q data leading to a trend of decreasing emittance with higher q at a fixed voltage for low ejection rates.

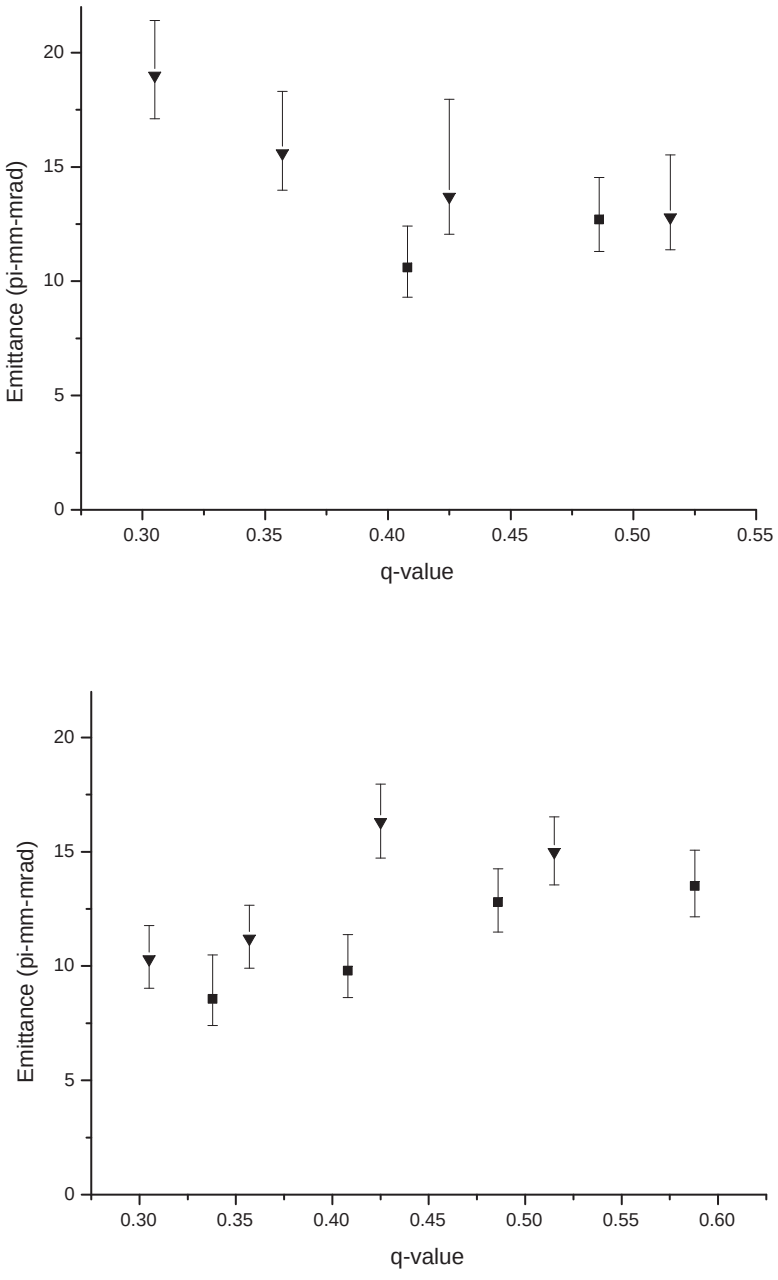

Figure 4–14: Effect of q value on emittance for 30 Hz ejection (top) and 90 Hz ejection (bottom). The data were taken at two constant RF voltages, 350 V (triangles) and 400 V (squares)

4.3.4 Cooling Time

To examine the effect of the cooling time (ie. the time required to cool the ions in the gas after they enter the RFQ device) on the emittance of the beam, two different times were considered. The first was the same as was used for the efficiency testing with continuous beam entering the RFQ and ejection occurring at a fixed rate to determine the cooling time that the ions spend in the trap. This will be the normal operating procedure when the RFQ is in use on the TITAN beam line and is shown in figure 4-15.

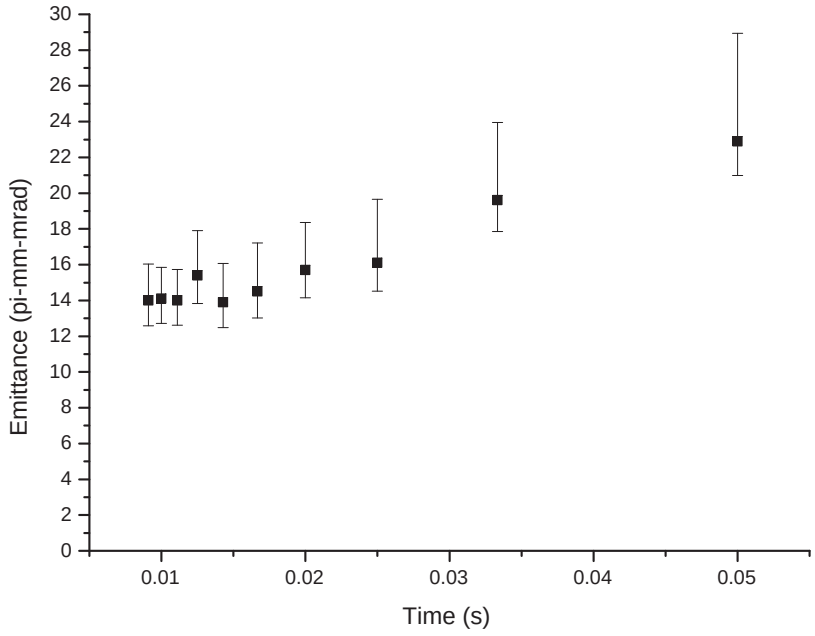

Figure 4–15: Emittance of extracted beam for ejection rates 20-100 Hz under normal operating conditions.

The emittance is constant for short cooling times less than 20 ms (f $>$ 50 Hz) and rises for longer cooling times. This is mainly due to the competing effects of the buffer gas cooling and the heating effects of other interactions. The ions interaction with each other increases with a larger number of ions

and this will increase their energy and the observed emittance. The incoming current in this case was 80 pA which means that at 80% efficiency $4x10^8$ ions entered the trap per second. At the lowest frequency rate of 20 Hz, $2x10^7$ ions entered the RFQ per bunch which is at the expected space charge limit of the RFQ in bunched mode ($2x10^7$ ions) [24]. This combines with the motion due to the RF confining field to produce an even larger effect. The plateau of the graph shows that the cooling time for the ions is relatively short and no gain is seen from longer cooling times.

For a more detailed study of the cooling behaviour of the ions, the emittance was also determined as a function of absolute cooling time with a pulsed beam so that all ions were in the trap for the same amount of time. This was done by building a simple gate circuit to put a voltage of 300V on one of the CB6 steerer electrodes before the deceleration plates. The potential was applied except during a 25 μs period. This deflected the beam away from the entrance to the RFQ when voltage was applied and only during the 25 μs period beam could enter the RFQ device. This also meant that the same number of ions were entering the device for all frequency settings and the data reflect the true effects of the time spent in the trap without the convolution of the ion density. The pulse was synchronised with the ejection pulse from the RFQ so that the window of beam into the RFQ occurred just after the ejection of the previous pulse.

Figure 4-16 shows the effect of changing frequency in this case. The data were taken with a helium gas pressure of 0.8 Pa and the incoming beam current was set so that 3.7 nA was exiting the source, corresponding to the number of ions entering the RFQ being $2x10^6$.

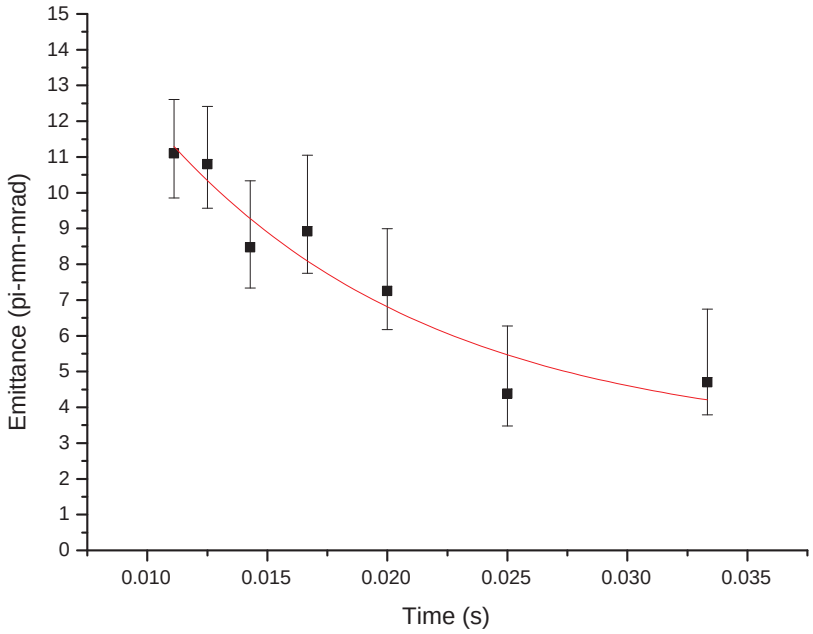

Figure 4–16: Emittance of extracted beam for ejection rates 30-90 Hz with chopped incoming beam.

A fit to the data gives a characteristic time of t = 11 ms (91 Hz). This is significantly higher than the simulated result of 600 μs [24] for a cooling time, owing largely to the lower gas pressure than the 2.5 Pa that was used for simulations. Also, the simulation was determining the time for the ions to reach thermal values using the relatively uncomplicated motion in the direction of the beam line. The true transverse motion inside the structure is complicated by the addition of the RF as well as the viscous drag model of the ion-gas interaction (see eqn 2-32). This would lead to longer time for cooling as the ions would be subject to forces that drive their motion as well as a retarding force.

CHAPTER 5
Conclusions and Future Outlook

5.1 RFQ Results and Conclusions

The RFQ has been fully commissioned off-line and demonstrated to operate as planned. The experimental data presented in the previous chapter has shown that ions can be efficiently transmitted to and through the RFQ and that the ion beam can be cooled, bunched and extracted.

We found that the efficiency of transporting ions into the RFQ from the 90 degree bender was 90 - 95% with operation at 30 kV. This is compared with the simulations that show 64% efficiency for the injection from the source. Most of the simulated losses came from matching of the ion source emittance to the injection optics and focusing parameters. The transfer efficiency of the post bend section was expected to be in the 97% range. We also found that transfer through the RFQ in DC mode with no trapping potentials applied gave an efficiency of 50 - 65% of the entering beam.

By determining the area of an integrated MCP signal through an RC circuit, we were able to determine the effect of varying certain parameters on the number of ions that were transported in bunched mode. It was established that a buffer gas pressure of at least 0.6 Pa was required to maximise the number of transmitted ions and that the trap depth needed to be between 16 and 20 Volts. It was also demonstrated that cooling times longer than 0.03 seconds decreases the efficiency of transport.

The tests also showed that the ions were being cooled and that the parameters of the RFQ affected their properties. It was found that the ions had lower emittances for very low gas pressure and for pressures above 0.9

Pa. This is in good agreement with the transmission efficiency and with the calculations which showed that a pressure of 1 - 2.5 Pa would be desirable. The effect of the q-value on the emittance of the beam was investigated and it was shown that higher RF voltage leads to lower emittances and that the ions are cooled more at q values close to 0.3. This is slightly different than the q = 0.39 optimum that was found in simulations due to the ion-ion interaction in conjunction with the ion-RF field interaction. It was also shown that the time required to cool the ions was 11 ms which is larger than simulated but is consistent with extrapolating to lower buffer gas pressures.

The lowest emittance found in these studies was 3.7 π-mm-mrad at extracted energy of 4 keV (as seen in figure 4-12). The best results in simulation yielded values of around 3 π-mm-mrad at 2.5 keV. To correct for the different energies, a transformation of the simulated result via equation 2.40 is performed such that

$$\epsilon_{4keV} = \epsilon_{2.5keV} \cdot \sqrt{\frac{4}{2.5}} \tag{5.1}$$

This gives an expected value at 4 keV of 3.8 π-mm-mrad, in agreement with observations.

5.2 TITAN Status and Plans

After the completion of these tests, the RFQ has been removed from the test stand and installed in the vertical section of the TITAN beam line. The optical elements are currently being installed and alignment has been completed (August, 2006). A redesigned deceleration system has been installed for injection into the RFQ. The new deceleration optics will use a conical injection electrode held at the same potential as the RFQ rather than two plates. The main motivation for the change is to eliminate the need for additional power supplies and wires close to the RFQ. This will reduce the possibility of

electrical sparking in the gas. In addition, the experimental beam line has increased differential pumping. These factors will enable the buffer gas pressure in the RFQ to be increased without increasing the risk of sparking or damage to components. Additional tests of RFQ performance can be done at higher pressures by mounting the emittance meter above the installed RFQ beam line.

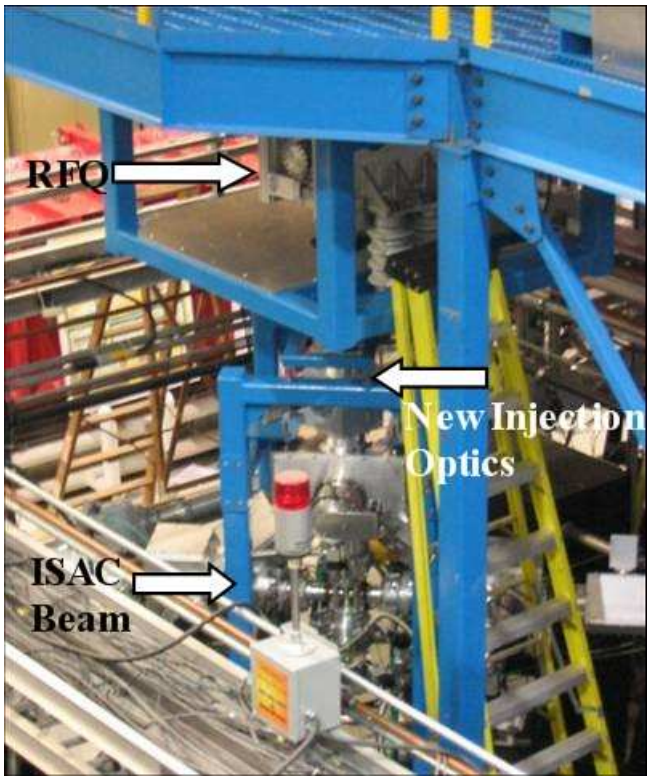

Figure 5–1: Current installation of RFQ (June 2006)

In situ testing of the RFQ is currently in progress. Testing for reverse extraction of the beam is planned in addition to transmission to the TITAN beam line. The reverse extraction will allow the cooled and bunched beam from the RFQ to be used in other experiments in the ISAC hall. These tests will be done with an off-line stable cesium surface ion source to determine

and maximise the performance of the RFQ and the transfer of ions to the remainder of the TITAN beam line.

The EBIT has been delivered to TRIUMF in April and is mounted on the platform. It will undergo further testing and optimisation as a unit before it is connected to the TITAN beam line in 2007.

The precision Penning trap magnet has been completed and machining is underway of the trap electrodes. The Penning trap and its associated electronics and supports are expected to be completed and installed in the Fall of 2006. The first online measurements of singly charged ions will be performed in December of 2006. Fully implementing the EBIT beam line and integrating the system for mass determination of highly charged ions will take place the following year.

APPENDIX A
Emittance Determination Program

The program for determining the emittance of the beam using a file consisting of an array of relative MCP signal strengths for each position and angle setting. The original program was written by R. Baartman and adapted for this set-up.

Emitmat.m

```
     plate_length = 69.85;
     plate_gap = 4.0;
     slit_width= 0.005;



if ~exist('pathname')
  display('Matlab script EMITMAT, written by R. Baartman, September, 2005');
   pathname=defpath;
   end;
if ~exist('fillast')
   fillast=0;
   end;
if ~exist('filename','var')
   pathpattern=sprintf('%s',pathname,'*.txt');
   [finamen pathnamen]=uigetfile(pathpattern,'Choose a scan file','location',[100,100]);
   if finamen ~= 0 finame=finamen;pathname=pathnamen;
   elseif ~exist('finame') finame=defname;pathname=defpath;
   end;
     filename=sprintf('%s',pathname,finame);
end;
if ~figflag(filename)
```

```
if ~exist('figpos') figpos=0;
  else figpos=figpos+500;end;
   figure('Name',filename,...
          'Position',[figpos,400,500,500],...
          'DefaultAxesFontName','times',...
          'defaultaxesfontsize',16);

   % Buttons
 callbackStr='clear filename;emitmat;';
 btnPos=[0 470 100 30];
 startHndl=uicontrol( ...
    'Style','pushbutton', ...
    'Position',btnPos, ...
    'backgroundcolor','green', ...
    'String','New File', ...
    'Interruptible','on', ...
    'Callback',callbackStr);
 callbackStr='checkifcurrent;M=rawM;sd=-1;processdata;';
 btnPos=[400 470 100 30];
 startHndl=uicontrol( ...
    'Style','pushbutton', ...
    'Position',btnPos, ...
    'backgroundcolor','cyan', ...
    'String','Recalculate', ...
    'Interruptible','on', ...
    'Callback',callbackStr);
 callbackStr='checkifcurrent;cutter;';
 btnPos=[300 0 200 30];
 startHndl=uicontrol( ...
    'Style','pushbutton', ...
    'Position',btnPos, ...
    'backgroundcolor',[1 0.65 0], ...
    'String','(1) Cut (Select Good Region)', ...
```

```
      'Interruptible','on', ...
      'Callback',callbackStr);
   callbackStr='checkifcurrent;erase;';
   btnPos=[0 0 200 30];
   startHndl=uicontrol( ...
      'Style','pushbutton', ...
      'Position',btnPos, ...
      'backgroundcolor',[1 0.75 0.8], ...
      'String','(2) Erase (Select Bad Region)', ...
      'Interruptible','on', ...
      'Callback',callbackStr);
   callbackStr='web helpem.html;';
   buttonStr='HOW';
   btnPos=[460 420 40 40];
   startHndl=uicontrol( ...
      'Style','pushbutton', ...
      'Position',btnPos, ...
      'backgroundcolor','red', ...
      'String',buttonStr, ...
      'Interruptible','on', ...
      'Callback',callbackStr);
end;


if ~strcmpi(filename,fillast)
     fid=fopen(filename);
     emittitle=fgetl(fid);
     disp('Filename = ');
     disp(filename);
     disp('Title = ');
     disp(emittitle);
     startposition=fscanf(fid,'%f',[1 1]);
     if size(startposition)==0. disp('Wrong file format!');return;end;
```

```
     stepsize=fscanf(fid,'%f',[1 1]);
     stepsize=stepsize*0.2; % stepsize is 0.2 mm
     if size(stepsize)==0. disp('Wrong file format!');return;end;
     v2=fscanf(fid,'%f',[1 1]);
     hv=fscanf(fid,'%f',[1 1])/1000.;
     if v2==0. disp('Plate Voltage is ZERO!');return;end;
     if hv==0. disp('Beam Energy is ZERO!');return;end;
     if stepsize==0. disp('Step Size is ZERO!');return;end;

     nvs=fscanf(fid,'%i',[1 1]);
     nps=fscanf(fid,'%i',[1 1]);
     if nps<3 disp('Not enough data');return;end;
     if nvs<3 disp('Not enough data');return;end;
     dum=fgetl(fid);
     dum2=fgetl(fid);
     rawM=fscanf(fid,'%f',[nps nvs]);
     th_conv = plate_length/plate_gap/2./hv/(nvs-1.)*v2;
     fclose(fid);
     M=rawM;sd=-1;
end;
processdata;
```

processdata.m

```
    x=(0:nps-1)*stepsize+startposition;
     th=(0:nvs-1)*th_conv;

peak=max(max(M));
kaep=min(min(M));
%Need some safeguards against min and max being isolated noise peaks.
```

```
while sum(sum(M<.1*peak+.9*kaep))==1
%If only one pt. below 10% of range...
  [i,j]=find(M==kaep);
%set it to the average of its neighbours
  M(i,j)=(M(1+mod(i-2,nps),j)+M(1+mod(i,nps),j)+ ...
               M(i,1+mod(j-2,nvs))+M(i,1+mod(j,nvs)))/4;
  kaep=min(min(M));
  end;
while sum(sum(M>.5*peak+.5*kaep))==1
%If only one pt. above 50% of range...
  [i,j]=find(M==peak);
%set it to the average of its neighbours
  M(i,j)=(M(1+mod(i-2,nps),j)+M(1+mod(i,nps),j)+ ...
               M(i,1+mod(j-2,nvs))+M(i,1+mod(j,nvs)))/4;
  peak=max(max(M));
  end;

  if peak==0 disp('data all ZERO');return;end;

  %Contour plot
ncontours=min(20,4*round(sqrt(sum(sum(M>(peak+kaep)/2)))));
if ncontours==0 ncontours=10;end;
lvls=kaep+(-0.9:ncontours)/ncontours*(peak-kaep);
display('Plotting. Please wait...');
[flag,fig]=figflag(filename);cla;
contourf(x,th,M',lvls);
xlabel('mm');
ylabel('mrad');
title(['EMIT. file: ' sscanf(finame, '%c', 11)],'Interpreter','none');
colormap(jet);

display('...Plotting done.');
```

```
     fillast=filename;
```

cutter.m

```
    disp('Select good region. Everything outside will be used to characterize noise.');
k = waitforbuttonpress;
figflag(filename);
point1 = get(gca,'CurrentPoint');    % button down detected
finalRect = rbbox;                   % return figure units
point2 = get(gca,'CurrentPoint');    % button up detected
point1 = point1(1,1:2);              % extract x and y
point2 = point2(1,1:2);
p1 = min(point1,point2);
inzxmin=max([1,1+round((p1(1)-startposition)/stepsize)]);
inzthmin=max([1,1+round(p1(2)/th_conv)]);
p2 = max(point1,point2);
inzxmax=min([nps,1+round((p2(1)-startposition)/stepsize)]);
inzthmax=min([nvs,1+round(p2(2)/th_conv)]);
inzzxmin=max([1,inzxmin]);
inzzxmax=min([nps,inzxmax]);
inzzthmin=max([1,inzthmin]);
inzzthmax=min([nvs,inzthmax]);
Z=rawM;
Z(inzzxmin:inzzxmax,inzzthmin:inzzthmax)=0.;
nzeroes=(inzzxmin-inzzxmax)*(inzzthmin-inzzthmax);
nonz=nps*nvs-nzeroes;
zset=sum(sum(Z))/nonz;

%Offset
M=rawM-zset;
```

```
Z=M;
Z(inzzxmin:inzzxmax,inzzthmin:inzzthmax)=0.;
sd=sqrt(sum(sum(Z.^2))/nonz);
zcut=1.5*sd;

%Cut
M=(M>=zcut).*M;

%get rid of isolated noise spikes
M=M.*(((roll(M,[ 1 0],'rot')==0)+...
       (roll(M,[-1 0],'rot')==0)+...
       (roll(M,[0  1],'rot')==0)+...
       (roll(M,[0 -1],'rot')==0)    )<3);

processdata;
rms;



erase.m

if sd<0 disp('You must run Cut first.');return;end;
disp('Select region to erase. Do this after selecting Good region.');
k = waitforbuttonpress;
figflag(filename);
point1 = get(gca,'CurrentPoint');    % button down detected
finalRect = rbbox;                   % return figure units
point2 = get(gca,'CurrentPoint');    % button up detected
point1 = point1(1,1:2);              % extract x and y
point2 = point2(1,1:2);
p1 = min(point1,point2);
inzxmin=max([1,1+round((p1(1)-startposition)/stepsize)]);
```

```
inzthmin=max([1,1+round(p1(2)/th_conv)]);
p2 = max(point1,point2);
inzxmax=min([nps,1+round((p2(1)-startposition)/stepsize)]);
inzthmax=min([nvs,1+round(p2(2)/th_conv)]);
inzzxmin=max([1,inzxmin]);
inzzxmax=min([nps,inzxmax]);
inzzthmin=max([1,inzthmin]);
inzzthmax=min([nvs,inzthmax]);
M(inzzxmin:inzzxmax,inzzthmin:inzzthmax)=0.;
processdata;
rms;
```

rms.m

```
%Profile vectors
xpro=sum(M')/nvs;
thpro=sum(M)/nps;
%
sx=sum(xpro);
sth=sum(thpro);
totsum=sum(sum(M));
if totsum==0. disp('data all ZERO: no stats');return;end;
  if sd~=0
  pfac=peak/sd;pinflate=pfac/(pfac-(1+log(pfac)))
  end;
x_bar=sum(xpro.*x)/sx;
th_bar=sum(thpro.*th)/sth;
xnew=x-x_bar;
thnew=th-th_bar;
x_2rms=2*sqrt(sum(xnew.^2.*xpro)/sx);
if x_2rms==0. disp(['WARNING: x-width is ZERO. Using step-size.' ...
                    ' Emittance will be an upper bound.'])
```

```
  x_2rms=stepsize;end;
x_or_y_mm_=x_2rms
th_2rms=2*sqrt(sum(thnew.^2.*thpro)/sth);
if th_2rms==0. disp(['WARNING: theta-width is ZERO. Using voltage' ...
                     ' step. Emittance will be an upper bound.']);
th_2rms=th_conv;end;
r12=thnew*M'*xnew'/x_2rms/th_2rms*4/totsum;
r_12_or_34=r12
waist=sqrt(1-r12^2)*x_2rms;
dis=r12*x_2rms/th_2rms;
emit_4rms=waist*th_2rms;
epsilon_pimum_=emit_4rms
%thwais=emit_4rms/x_2rms;
%alpha=-r12/sqrt(1-r12^2);
%betat=x_2rms^2/emit_4rms;

phi=[0:1:360]*pi/180;
th_ell=sin(phi);
x_ell=cos(phi)*waist+x_bar;
x_ell=x_ell+dis*th_2rms*th_ell;
th_ell=th_ell*th_2rms+th_bar;
figflag('Contour');hold on;
plot(x_ell,th_ell,'w','LineWidth',2);
set(gcf,'DefaultTextFontName', 'Times','DefaultTextFontSize',12);

text(.0,.1,[' x_{2rms}= ' num2str(x_2rms,4) ' mm'],'Units', ...
     'normalized','Color','white');
text(.0,.05,[' \theta_{2rms}= ' num2str(th_2rms,4) ' mrad'],'Units', ...
     'normalized','Color','white');
text(.3,.1,[' r_{12}   = ' num2str(r12,4)],'Units', ...
     'normalized','Color','white');
text(.3,.05,['\epsilon_{2rms}= ' num2str(emit_4rms,3) ' \pi\mum'],'Units', ...
     'normalized','Color','white');
```

```
text(.6,.05,['Inflate Factor= ' num2str(pinflate) ' '],'Units', ...
     'normalized','Color','white');
```

APPENDIX B
Abbreviations Used in This Work

The following is a list of the abbreviations used in the text.

CKM	Cabibbo Kobayashi Maskawa matrix
DC	Direct Current (non oscillating)
DTL	Drift Tube Linac
EBIT	Electron Beam Ion Trap
FET	Field Effect Transistor
ISAC	Ion Separation OnLine
HV	High Voltage
LEBT	Low Energy Beam Transport
MCP	microchannel plate
MOSFET	Metal Oxide Semiconductor Field Effect Transistor
PVC	Polyvinyl Chloride plastic
RF	Radio Frequency
RFQ	Radio Frequency Quadrupole
TITAN	TRIUMF's Ion Trap for Atomic and Nuclear science
TOF	Time Of Flight method
TRIUMF	TRI-University Meson Facility
TTL	Transistor-Transistor Logic

References

[1] R. Laxdal, R. Baartman, P. Bricault, et al. Status of the ISAC Accelerator for Radioactive Beams. *Linac98 Proceedings*, page 786, 1998.

[2] B. Martin and G. Shaw. *Particle Physics*. John Wiley & Sons, 1997.

[3] Bret A et al. Updated Results on the CKM Matrix and the Unitary Triangle. *Eur. Phys. J.*, 41:1, 2005.

[4] W. Menges. Measurement of the CKM Matrix Elements V_{cb} and V_{ub} at the B Factories. *Proceedings of the 14th Int. Workshop on Deep Inelastic Scattering*, 2006.

[5] G. Savard, F. Buchinger, J. Clark, et al. Q Value of the Superallowed Decay of ^{46}V and its Influence on V_{ud} and the Unitarity of the Cabibbo-Kobayashi-Maskawa Matrix. *Phys. Rev. Lett.*, 95, 2005.

[6] J. Hardy and I. Towner. Superallowed $0^+ \rightarrow 0^+$ Beta-Decay and CKM Unitarity. *Eur. Phys. J. A*, 15:223, 2002.

[7] J. Dilling, P. Bricault, M. Smith, et al. The Proposed TITAN Facility at ISAC for Very Precise Mass Measurements on Highly Charged Short-Lived Isotopes. *Nucl. Instr. and Meth. B*, 204:492, 2003.

[8] M. Froese. The TITAN Electron Beam Ion Trap: Assembly, Characterization, and First Tests. Master's thesis, University of Manitoba, 2006.

[9] G. Sikler, J. Crespo Lopez-Urrutia, J. Dilling, et al. A High-Current EBIT for Charge-Breeding of Radionuclides for the TITAN Spectrometer. *Eur. Phys. Journal A*, 25:63, 2005.

[10] V. Ryjkov, L. Blomeley, M. Brodeur, et al. Titan Project Status Report and a Proposal for a New Cooling Method of Highly Charged Ions. *Eur. Phys. Journal A*, 25:53, 2005.

[11] H. Dehmelt and F. Walls. Bolometric Technique for the RF Spectroscopy of Stored Ions. *Phys. Rev. Lett.*, 21:127, 1968.

[12] W. Paul. Electromagnetic Traps for Charged and Neutral Particles. *Reviews of Modern Physics*, 62:531, 1990.

[13] Nobel Prize in Physics Press Release, 1989.

[14] F. Major and H. Dehmelt. Exchange Collision Technique for the RF Spectroscopy of Stored Ions. *Phys. Rev.*, 170:91, 1968.

[15] G. Savard, R. Barber, C. Boudreau, et al. The Canadian Penning Trap Spectrometer at Argonne. *Hyperfine Interactions*, 132:221, 2001.

[16] L. Brown and G. Gabrielse. Geonium Theory: Physics of a Single Electron or Ion in a Penning Trap. *Rev Mod Phys*, 58:223, 1986.

[17] M. Konig, G. Bollen, H. Kluge, et al. Quadrupole Excitation of Stored Ion Motion at the True Cyclotron Frequency. *International Journal of Mass Spectrometry and Ion Processes*, 142:95, 1995.

[18] J. Clark, G. Savard, K. Sharma, et al. Precise Mass Measurement of ^{68}Se, a Waiting-Point Nuclide Along the RP Process. *Phys Rev Letters*, 92:192501, 2004.

[19] A. Jokinen, J. Huikari, V. S. Kolhinen, et al. The First Cooled Beams from JYFL Ion Cooler and Trap Project. *Nuclear Physics A*, 701:557, 2002.

[20] P. Dawson. *Quadrupole Mass Spectrometry and its Applications*. Elsevier Scientific, 1976.

[21] I. Dayton, F. Shoemaker, and R. Mozley. The Measurement of Two Dimensional Fields. Part II: Study of a Quadrupole Magnet. *Rev. Sci. Instr.*, 25:485, 1954.

[22] R. March. An Introduction to Quadrupole Ion Trap Mass Spectrometry. *Journal of Mass Spectrometry*, 32:351, 1997.

[23] J. Richards et al. A New Operating Mode for the Quadrupole Mass Filter. *Int. J. of Mass Spectrometry and Ion Phys.*, 12:239, 1973.

[24] M. Smith. A Square-Wave-Driven Radiofrequency Quadrupole Cooler and Buncher for TITAN. Master's thesis, University of British Columbia, 2005.

[25] O. Gianfrancesco. Design Principles of a High Field RFQ Device for Ion Cooling and Confinement. Master's thesis, McGill University, 2002.

[26] O. Hadary, M. Barnes, and G. Wait. Capacitance of TITAN RFQ Driver and RFQ Structure, Extraction Electrode Considerations, and Power Dissipation in the Driver. *TRIUMF Design Note*, 2004.

[27] T. Kim. *Buffer Gas Cooling of Ions in a Radio Frequency Quadrupole Ion Guide*. PhD thesis, McGill University, 1997.

[28] H. Ellis, E. McDaniel, D. Albritton, et al. Transport Properties of Gaseous Ions Over a Wide Energy Range. *Atomic Data and Nuclear Data Tables*, 22:180, 1978.

[29] M. D. N. Lunney, R. Moore, and F. Buchinger. The Temperature of Buffer Gas Cooled Ions in a Paul Trap. *Journal of Modern Optics*, 39:349, 1992.

[30] H. Wollnik. *Optics of Charged Particles*. Academic Press Inc., 1987.

[31] Heat Wave Labs, www.cathode.com/i_alkali.htm.

[32] M. Barnes and G. Wait. A 25 kV, 75 kHz Kicker for Measurement of Muon Lifetime. *Pulsed Power Conference Proceedings*, 2003.

[33] RF Power Transistors and Diodes, http://www.ixysrf.com/.

[34] M. Barnes, O. Hadary, and G. Wait. A High Frequency MOSFET Driver for the TITAN Facility at TRIUMF. *Pulsed Power Conference Proceedings*, 2005.

[35] F. Herfurth, J. Dilling, et al. Linear radiofrequency ion trap for accumulation, bunching and emittance improvement of radioactive ion beams. *Nuclear Physics A*, 469:254, 2001.

[36] J. Wiza. Microchannel Plate Detectors. *Nuclear Instruments and Methods B*, 162:587, 1979.

[37] P. Allison, J. Sherman, and D. Holtkamp. An Emittance Scanner for Low Energy Ion Beams. *IEEE Trans Nucl*, 4:2204, 1983.

[38] Simion 3D Ion and Electron Optics Simulator, www.simion.com.